AD-780 428

COMPUTATION OF THE RESIDUAL RADIATION
TRANSMISSION FACTOR FOR THE MARINE
CORPS LVTP7

Robert G. Cawley

Naval Ordnance Laboratory
White Oak, Maryland

28 September 1973

REPORT DOCUMENTATION PAGE		READ INSTRUCTIONS BEFORE COMPLETING FORM
1. REPORT NUMBER NOLTR 73-137	2. GOVT ACCESSION NO.	3. RECIPIENT'S CATALOG NUMBER AD-780428
4. TITLE (and Subtitle) COMPUTATION OF THE RESIDUAL RADIATION TRANSMISSION FACTOR FOR THE MARINE CORPS LVTP7		5. TYPE OF REPORT & PERIOD COVERED Final
		6. PERFORMING ORG. REPORT NUMBER
7. AUTHOR(s) Robert G. Cawley		8. CONTRACT OR GRANT NUMBER(s)
9. PERFORMING ORGANIZATION NAME AND ADDRESS Naval Ordnance Laboratory Silver Spring, Maryland 20910		10. PROGRAM ELEMENT, PROJECT, TASK AREA & WORK UNIT NUMBERS 30111 NOL 814/NOL
11. CONTROLLING OFFICE NAME AND ADDRESS Marine Corps Development & Education Center Quantico, Virginia 22134 (Major Gapinski)		12. REPORT DATE 28 September 1973
		13. NUMBER OF PAGES 52
14. MONITORING AGENCY NAME & ADDRESS(If different from Controlling Office)		15. SECURITY CLASS. (of this report) UNCLASSIFIED
		15a. DECLASSIFICATION/DOWNGRADING SCHEDULE

16. DISTRIBUTION STATEMENT (of this Report)

Approved for Public Release; distribution unlimited

17. DISTRIBUTION STATEMENT (of the abstract entered in Block 20, if different from Report)

18. SUPPLEMENTARY NOTES

19. KEY WORDS (Continue on reverse side if necessary and identify by block number)

Shielding	Radiation reduction factor
Radiation protection	Gamma-ray transmission
Armored vehicle	Buildup factor
Fallout	Ground roughness
Protection factor	

20. ABSTRACT (Continue on reverse side if necessary and identify by block number)

We develope an analytical technique for computing the gamma radiation reduction factor for a slab of arbitrary orientation in a field of uniformly distributed radioactive fallout (CO^{60}). We apply this to a model of the army M113 APC, assuming the entire reduction is due to material in the vehicle walls, ceiling and floor. The resulting protection, $P = 1.5$, differs sharply with the measured value, $P = 4.0$, which we assume is due to the presence of other material than that in the vehicle surfaces. As a second model of the M113 we assume its shape

DD FORM 1473 EDITION OF 1 NOV 65 IS OBSOLETE
1 JAN 73

S/N 0102-014-6601 |

20.

Abstract; (cont'd)

to be that of a parallelepiped having a square verticle cross section of side L, uniform wall thickness t_{eff} and height equal to the actual vehicle height. We choose L and t_{ff} so that the surface area and total mass of the model vehicle agree with those of the actual vehicle. A 10% albedo correction to the protection then results in agreement with experiment: $R_{theory}^{M113} = 3.9$. We apply the same approach to the LVTP7, getting $R_{theory}^{LVTP7} = 4.1$. The radiation reduction factors, $R = P,^{-1}$ for these two cases are 0.26 and 0.24 respectively; and the residual radiation transmission factors, defined from R to include the effects of a ground roughness parameter of 3 ft, are both 0.3.

The analytical method also should be useful to save computation time and cost in numerical work.
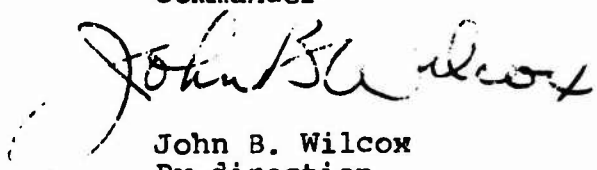
Computation of the

Residual Radiation Transmission Factor for

the Marine Corps LVTP7

by

Robert G. Cawley

We develope an analytical technique for computing the gamma radiation reduction factor for a slab of arbitrary orientation in a field of uniformly distributed radioactive fallout (Co^{60}). We apply this to a model of the army M113 APC, assuming the entire reduction is due to material in the vehicle walls, ceiling and floor. The resulting protection, $P = 1.5$, differs sharply with the measured value, $P = 4.0$, which we assume is due to the presence of other material than that in the vehicle surfaces. As a second model of the M113 we assume its shape to be that of a parallelepiped having a square vertical cross section of side L, uniform wall thickness t_{eff} and height equal to the actual vehicle height. We choose L and t_{eff} so that the surface area and total mass of the model vehicle agree with those of the actual vehicle. A 10% albedo correction to the protection then results in agreement with experiment: $R_{theory}^{M113} = 3.9$. We apply the same approach to the LVTP7, getting $R_{theory}^{LVTP7} = 4.1$. The radiation reduction factors, $R = P^{-1}$ for these two cases are 0.26 and 0.24 respectively; and the residual radiation transmission factors, defined from R to include the effects of a ground roughness parameter of 3 ft, are both 0.3.

The analytical method also should be useful to save computation time and cost in numerical work.

NOLTR 73-137

Computation of the Residual Radiation Transmission Factor for the
Marine Corps LVTP7.

This report gives a new method for calculating the γ-radiation
transmission through a plane slab of arbitrary orientation, above a
field of uniformly distributed radioactive fallout. The method is
applied to the Marine Corps LVTP7 to estimate the residual radiation
transmission factor. The work was sponsored by the U. S. Marine
Corps Development and Education Command.

ROBERT WILLIAMSON II
Captain, USN
Commander

John B. Wilcox
By direction

TABLE OF CONTENTS

ILLUSTRATIONS

TABLES

I. INTRODUCTION

The present work reports the results of an effort to compute the protection factor and the residual radiation transmission factor (RRTF:defined in Section 2) for the Marine Corps LVTP7 troop carrier in a field of radioactive fallout. The P7 is similar to another vehicle, the army M113 APC (armored personnel carrier), for which experimental data are available,[1] and we have used those results in our method. Briefly, we have developed an approximate analytical technique, which enables us to calculate the protection factor for an enclosure whose walls are composed of plane slabs having arbitrary orientations.

Applied to a fairly faithful model of the M113 geometry and using for wall thicknesses the actual values, the calculated value of the protection factor is P = 1.53, much lower than the experimental value of 4.0. The reason for this discrepancy is that the mass of the M113 in the model is less than half the mass of the actual vehicle in the (combat loaded) experimental conditions, so there is quite a bit more "extra" material actually present to enhance the protection over that afforded by the model; this material includes the engine, treads, wheels, axles, fuel, troops, interior panelling surfaces, and sundry paraphernalia, the mass distribution of which it is impractical to try to take into account. In the first place the labor involved would be enormous, and the results withal probably not trustworthy. Even more significantly, there is a "theoretical error" inherent in the notion of vehicle protection factor, a circumstance which makes too precise a result meaningless: the actual protection factor varies from place to place inside the vehicle owing to the irregular mass distribution (including shape), and to dependence of the radiation source intensity on height above the ground. Variations arising from these, and other effects as well, are at least 10 - 15%, experimentally,[1] so the complexity of the actual circumstances has the effect of easing the calculational problem.

To deal with the problem of the extra mass we have idealized the actual vehicle by a rectangular parallelepiped with square shape and having height equal to that of the actual vehicle. The wall thickness and the size of the square were fixed by requiring equality between the masses and surface areas of the actual vehicle and the model vehicle. The equation of the protection factor has an especially simple approximate form for this geometry, and the results we have obtained are in good agreement with experiment. Eqs. (6.18) and (6.17) give the values reported in Reference 1, respectively, for the "survey correlation factor," which, for the

1

experimental conditions of ground roughness, was .86 times the protection factor, and the calculated results from our model, which assumes a 10% albedo contribution to the reduction factor.

The results for the P7, modeled in this way, as a square rectangular parallelpiped, are given in Section 6 (eqs. (6.20) and (6.22)).

The outline of the report is this. In Section 2 we establish the character of the physical approach we have adopted, present source and buildup data, motivate our choice for ground roughness parameter, and give the general expressions of the protection factor, the survey correlation factor and the RRTF. In Section 3 we explicate the geometrical problem of the reduction factor (unscattered component) for a plane slab of arbitrary orientation, introducing a certain shape approximation which exploits essential features of the source. In Section 4 we develope the principal analytical formulas for the slab reduction factor and solid angle factor. In Section 5 we present the results of the M113 model calculation which neglects the "extra matter" actually present but not contained in the walls. In Section 6 we present details of the parallelepiped model and give results for both the M113 and the P7. In Section 7 we discuss the results, and in Section 8 we give a brief summary of what we have done and offer a concluding remark concerning application of our method to computer programing.

2. PRELIMINARY CONSIDERATIONS

A. Physical Approach

We assume the exposure at a point inside the vehicle to be
a sum of contributions from all directions, with that from any given
direction expressed as the product of a buildup factor with the
exponentially attenuated unscattered component deriving from an
assumed angular dependent source. For the source distribution we
assume a form derived from curves given by Spencer,[2] for air,
above an infinite plane of uniformly distributed fallout, simulating
effects of ground roughness by using an effective height above the
ground which is augmented by an amount Δh over the actual height.[2]
The normalization of the angular distribution, $\ell(h,x)$, where
$x = \cos \theta$, θ the angle of the line of sight from the detector
position, of the incident γ ray with the downward vertical, is set by
the usual condition,

$$L(h) = \int_{-1}^{+1} d x \, \ell(h,x) = 1, \text{ for } h = 3 \text{ feet} \tag{2.1}$$

To neglect of albedo, the reduction factor for detector height
h ($h_{eff} = h + \Delta h$ if there is ground roughness) due to a slab of
thickness t_i and surface Σ_i
is

$$r_i = r_{\Sigma_i}(h) = B_0(t_i) E_{\Sigma_i}(h,t_i) \tag{2.2}$$

where $B_0(t_i)$ is the buildup factor for the given slab material,
whose thickness is t_i, and $E_{\Sigma_i}(t_i)$ is[3]

$$E_{\Sigma_i}(h,t_i) = \frac{1}{2\pi} \int d\Omega g_{\Sigma_i}(\Omega) \ell(h,\cos\theta) \exp(-\mu_{\Sigma_i} t_{\Sigma_i} \sec\beta\theta_0), \tag{2.3}$$

where μ_Σ is the inverse attenuation length for the substance of
which Σ is composed, θ_0 is the angle formed by the incident γ-ray
and the normal to Σ, β is the so-called refraction parameter, which
depends on the slab material,[3] and the "step" function $g_\Sigma(\Omega)$ is
unity if the line of sight of the direction indicated by Ω
intersects Σ, and is zero otherwise. In the same spirit the re-
duction factor inside the enclosure, at height h--above the ground
is understood--is

$$\Re(h) = aR = a\sum_i r_{\Sigma_i}(h_{eff}), \tag{2.4}$$

where the summation extends over all the surfaces of the enclosure.
In eq. (2.4) we have included an overall factor $\underline{a}$ to account for
albedo, i.e. the contribution to the exposure from γ rays back-
scattered from the interior faces of the enclosure. The protection
factor within the enclosure at height h is defined by

3

$$P(h) = L(3 \text{ feet})\, \mathcal{R}^{-1} = \mathcal{R}^{-1}, \tag{2.5}$$

by eq. (2.1); it is the ratio of the exposure in the
standard unprotected position (3 feet above a smooth infinite plane
of uniformly distributed fallout) to the exposure at height h
within the enclosure under (assumed) given ground roughness con-
ditions. The survey correlation factor, S, reported in Reference
1, is a similar ratio, with the <u>measured</u> exposure at h = 3 feet
replacing that for the standard unprotected position; so

$$S(h) = L(3 \text{ feet} + \Delta h)\, \mathcal{R}^{-1} = L(3 \text{ feet} + \Delta h)P. \tag{2.6a}$$

Since L(h), defined in eq. (2.1), is a decreasing function of h,
S(h) is smaller than P(h). We define the RRTF to be S^{-1}:

$$RRTF \equiv S^{-1}. \tag{2.6b}$$

B. <u>The Source</u>

If the source were that due solely to unscattered γ-rays of
energy E, we would have

$$\ell(h,x) = c\, x^{-1} \exp(-\mu_a h x^{-1}), \quad x>0, \tag{2.7}$$
$$\ell(h,x) = 0 \quad\quad\quad x<0,$$

where μ_a^{-1} is the γ-ray attenuation length in air for energy E, and
c is a normalization coefficient. In Figures 1 and 2 we have re-
produced two of the curves from Reference 2, plots of $\ell(h,x)$ for
h = 6.6 feet and h = 66 feet, together with plots of eq. (2.7) for
values of μ_a such that the location of the peaks of the former co-
incide with those of the latter, which occur at

$$x = \mu_a h \equiv \varkappa, \tag{2.8}$$

and with normalization of (2.7) chosen so that the heights of the
peaks coincide. For h = 6.6 feet the agreement for x > 0 is
extremely good and for h = 66 feet the disagreement is of order 10%,
or so. Our interest is in height values appropriate to the 6.6 feet
case.

To very good accuracy, to quite a bit better than 5% for heights
of interest to us, we are justified in using the form (2.7) for
x > 0. For the skyshine part, x < 0, we assume a parabola centered
at x = -1,

$$\ell(h,x) = c_1 + c_2 (x+1)^2, \tag{2.9}$$

requiring the constants c_1 and c_2 to be chosen so that
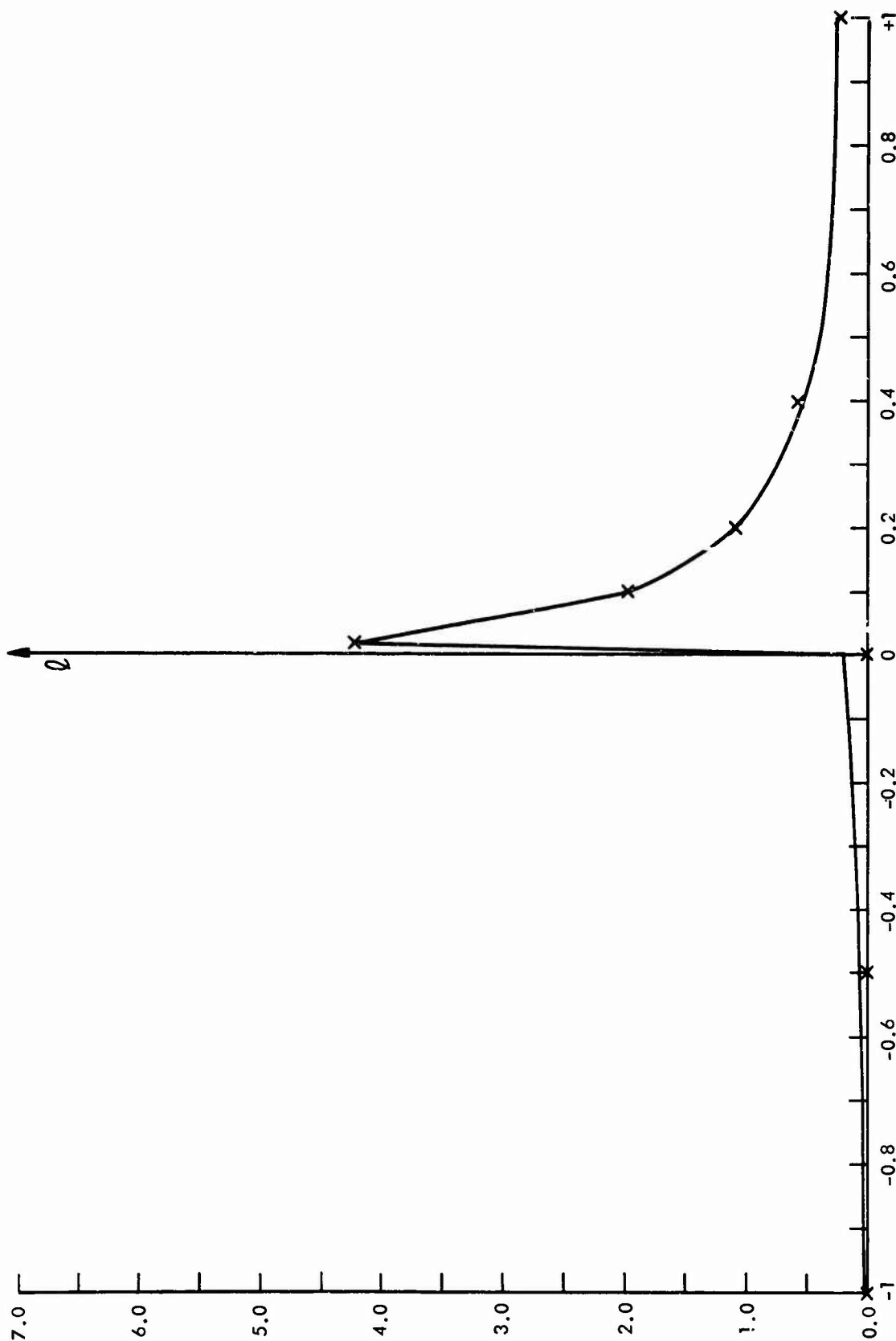
$$\ell(h,-1)/\ell(h,0) = .195 \tag{2.10}$$

4

FIG. 1   Exposure angular distribution ($x = \cos\theta$) above an infinite plane of radioactive fallout. Solid curve (taken from reference 2): in water, scaled to air, height 6.6 ft.; 1.12 hr. fission spectrum. The crosses show the function given in eq. (2.7), with $h = 6.6$ ft., and μ_a and c chosen so that the peak of the corresponding curve coincides with the peak of the curve drawn in the figure.
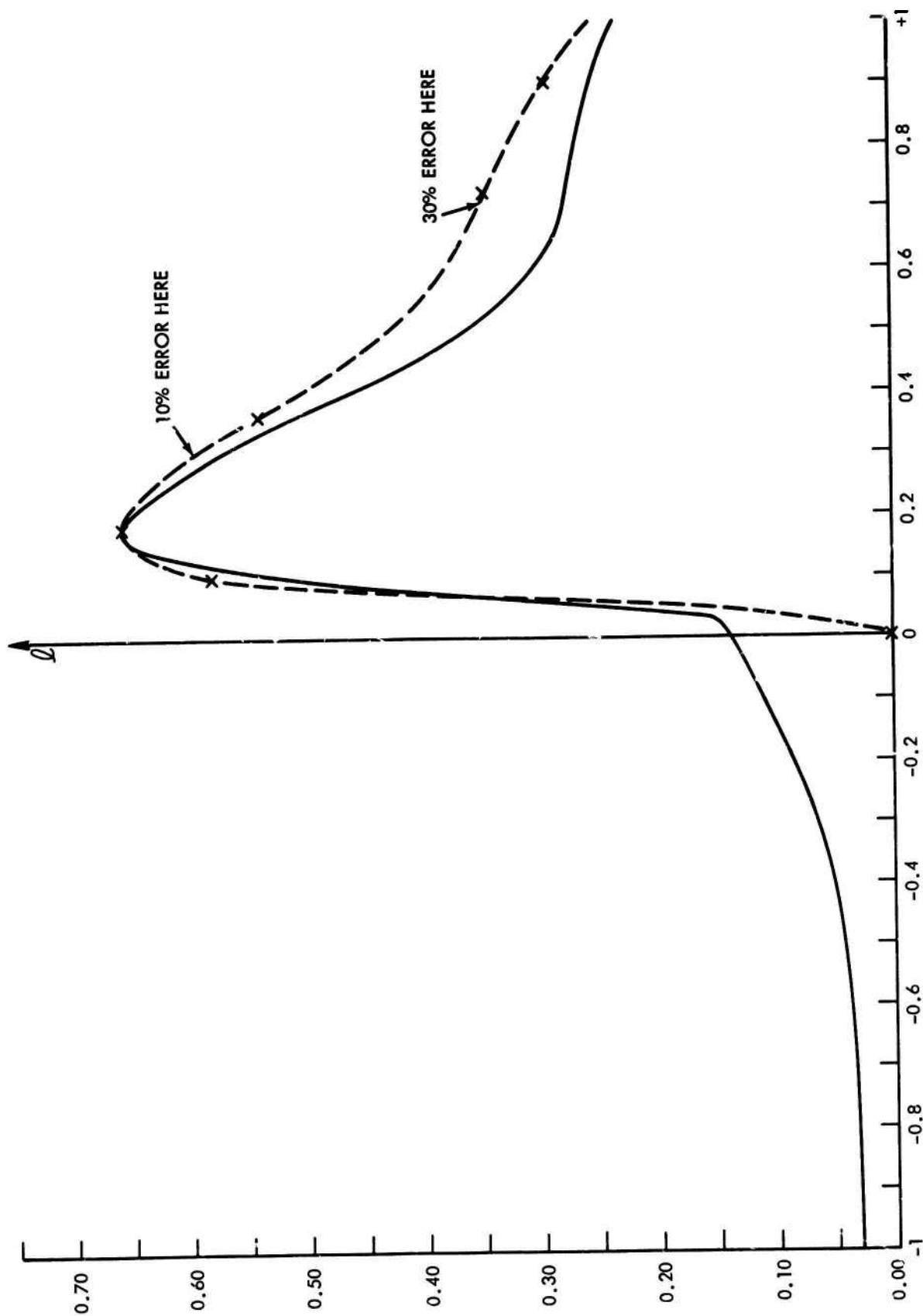
5

FIG. 2 Same as FIG. 1, but with h = 66 ft. Here the crosses have been joined by a dashed curve.

which is good to <5% between h = 3.3 feet and h = 33 feet. We fix the relative normalization between the x < 0 and x > 0 parts by requiring

$$S = .110L, \tag{2.11}$$

where

$$S = \int_{-1}^{0} dx\, \ell(h,x), \tag{2.12}$$

is the skyshine contribution to L. Between 3 feet and 33 feet S rises from .093L to .125L, from curves in Reference 2; interpolation gives S = .105L for h = 6.6 feet, while direct measurements from Figure 1 have given us eq. (2.11).

The normalization coefficient c, in eq. (2.7), still remains to be fixed; it is a buildup factor, and it depends on h. Also, we need to choose a value for μ_a. First the latter: the contribution to L from x > 0, assuming the form in eq. (2.7), is $cE_1(\varkappa)$ where $E_1(\varkappa)$ is the exponential integral,

$$E_1(\varkappa) = \int_{\varkappa}^{\infty} dy\, y^{-1} \exp(-y); \tag{2.13}$$

we equate this at h = 6.6 feet to

$$L(6.6 \text{ feet}) - S(6.6 \text{ feet}) = .890L(6.6 \text{ feet}),$$

taking L(6.6 feet) = .87 from Spencer[2], to get

$$c(6.6 \text{ feet})E_1(\varkappa(6.6 \text{ feet})) = .774. \tag{2.14}$$

But, with $x = \varkappa$ locating the peak, we have also

$$c \cdot (e\varkappa)^{-1} = \ell_p \tag{2.15}$$

where ℓ_p is the peak value of ℓ, which is 4.15 for h = 6.6 feet; combining these gives

$$\varkappa E_1(\varkappa)\big|_{6.6 \text{ feet}} = .774 \cdot (4.15e)^{-1} = .0686, \tag{2.16}$$

whose solution is $\varkappa = .0207$ (to about 3%), so that*

$$\mu_a^{-1} = 6.6 \text{ ft.} \div .0207 = 319 \text{ feet, or } 97m,$$

$$\mu_a = .003134 \text{ ft.}^{-1} \tag{2.17}$$

---

* The value 97m seems a little low for the spectrum from which Spencer's curves are calculated; this was a 1.12 hr. fission spectrum, for which, using spectrum data given in Reference 2, we have estimated μ_a^{-1} ≈ 123m, to perhaps 15%.

If we use eq. (2.15), taking $x = \mu_a h$ and reading l_p from Spencer's curves, we obtain a set of values of c_p which can be fit with a straight line

$$c = .2169 + .835\, x, \quad 4 \text{ ft} \leq h \leq 42 \text{ ft.,} \tag{2.18}$$

while for h = 3 ft. we get

$$c(3 \text{ ft.}) = .2172 \tag{2.19}$$

From eqs. (2.10), (2.11) and (2.18) we obtain c, and c_2, and with this the complete form for $l(h,x)$,

$$l(h,x) = c \cdot \begin{cases} x^{-1}\exp(-\mu_a h x^{-1}), & x > 0, \\[2mm] .264E_1(\mu_a h)[.195 + .805\,(x+1)^2], & x < 0. \end{cases} \tag{2.20}$$

This can be used for 4 ft. $\leq h \leq 42$ ft. even though (2.10) and (2.11) weaken above 30 ft., for the whole skyshine contribution is not much more than 15 to 20% of the total below h = 42 ft. When we integrate (2.20) using (2.19), we find $L(3 \text{ ft.}) = 1.000$.

The source function, eq (2.20), is not quite what we want, however. We need to shift the value of μ_a if we wish to compare with experiments of Reference 1, where Co[60] was used as the γ-ray source. The Co[60] spectrum contains two principle peaks, at 1.17 MeV and 1.33 MeV. If we idealize this as a single peak at 1.25 MeV, the attenuation length in air is

$$\mu_a^{-1} = \frac{A}{z} \cdot \rho^{-1}\, \frac{m_p}{f(E)\sigma_{th}} \tag{2.21}$$

where A/z = 2 is the atomic weight to number ratio for air, $\rho = 1.312 \times 10^{-3}$ gm/cm^3 is the density of air (STP), m_p the mass of the proton, σ_{th} the Thompson cross section,

$$\sigma_{th} = \frac{8\pi}{3} r_o^2, \quad r_o = e^2/m_e c^2 = \text{classical electron radius,}$$

and f(E) is the Compton cross section for γ energy E, in units of[4] σ_{th}. We get

$$\mu_a^{-1}(1.25 \text{ MeV}) = 131.7 \text{ m} = 431 \text{ ft}$$
$$\mu_a = .002314 \text{ ft}^{-1}, \tag{2.22}$$

which are somewhat different from the values appearing in (2.17).

To convert to the Co^{60} spectrum, we simply take over eq. (2.20), regarding the right side as a function of $\varkappa = \mu_a h$, valid between $\varkappa_1 = .003134$ ft^{-1} x 4 ft = .01254, and $\varkappa_2 = .003134$ ft^{-1} x 42 ft = .1316, where the $\varkappa$ dependence of c is indicated by eq. (2.18). There is an overall normalization change affecting the coefficients in eq. (2.18), however, arising from the fact that the normalization condition, eq. (2.1), holds for any μ_a. We have, at h = 3 ft.,

$$c(3 \text{ ft, } .002314 \text{ ft}^{-1}) \equiv N \cdot c(3 \text{ ft, } .003134 \text{ ft}^{-1}) \qquad (2.23a)$$

while from eqs. (2.1) and (2.20) with $\mu_a = .002314$ ft^{-1},

$$c(3 \text{ ft, } .002314 \text{ ft}^{-1}) \times 1.1222 \, E_1 \, (.006942) = 1 \qquad (2.23b)$$

whence

$$N = .938 \qquad (2.24)$$

We assume that the same factor scales the source to the new value of μ_a for other values of h and we get

$$c = .2034 + .783\mu_a h, \qquad 5.5 \text{ ft.} < h < 55 \text{ ft.,}$$

$$= .2038, \qquad h = 3 \text{ ft.} \qquad (2.25)$$

The limits of validity to (2.25) are determined as $\varkappa_1/\mu_a$ and $\varkappa_2/\mu_a$ (compare eq. (2.18)).

Summarizing, the source is given in eqs. (2.20) and (2.25), for the case of a Co^{60} source.

C. Buildup Factor for Transmission through a Wall.

Taking the data of Reference 3, we can fit the buildup factor, as a function of (normal) wall thickness, to a straight line. For X out to 2 mean free paths (which is all we need) we have, for concrete, or aluminum

$$B_o = 1 + .76X, \qquad (2.26)$$

when X is the mass thickness in units of μ^{-1}. For aluminum, using eq. (2.21) with $\rho = 2.72$ gm/cm^3, we have $\mu^{-1} = \mu_{A\ell}^{-1} = 2.60$ in, so that

$$B_o = 1 + .292 \, t \qquad (2.27)$$

where t is the wall thickness in inches. This is good to a percent or so.

9

D. Ground Roughness

The data of Reference 1 permit the determination of the ground roughness parameter, Δh, which existed under the conditions of the experiment. Figure 3 shows a plot of the reported unprotec-ted exposure as a function of height h, normalized to unity at 3 feet, and Figure 4 shows four theoretical curves of $L(h+\Delta h)$, for $\Delta h = 0,3,6$, and 9 feet, with zeros of ordinate chosen so that all curves pass through the same point at h = 3 feet. When the two figures are superposed, the experimental curve lies on top of the theoretical curve having Δh = 3 feet. For comparison purposes therefore we adopt this value for the ground roughness parameter throughout. We notice that if h < 5 feet then $\kappa < .002314 \times (5+3) = .0185 << 1$, a fact we exploit below.
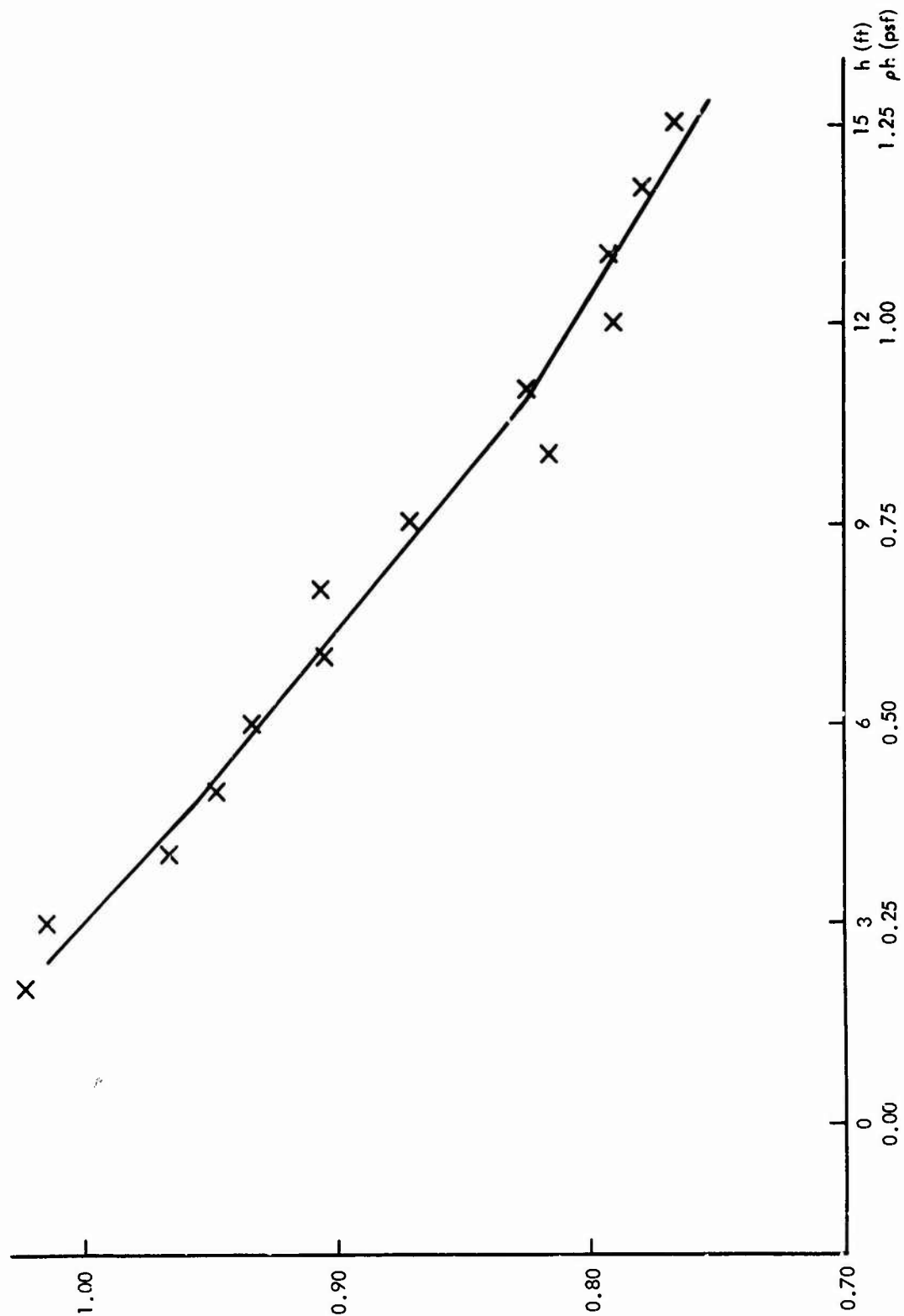
FIG. 3 Measured unprotected total exposure dose reported in reference 1, as a function of actual height above ground, and normalized (arbitrarily) to one, at 3 ft. (Co^{60} source).
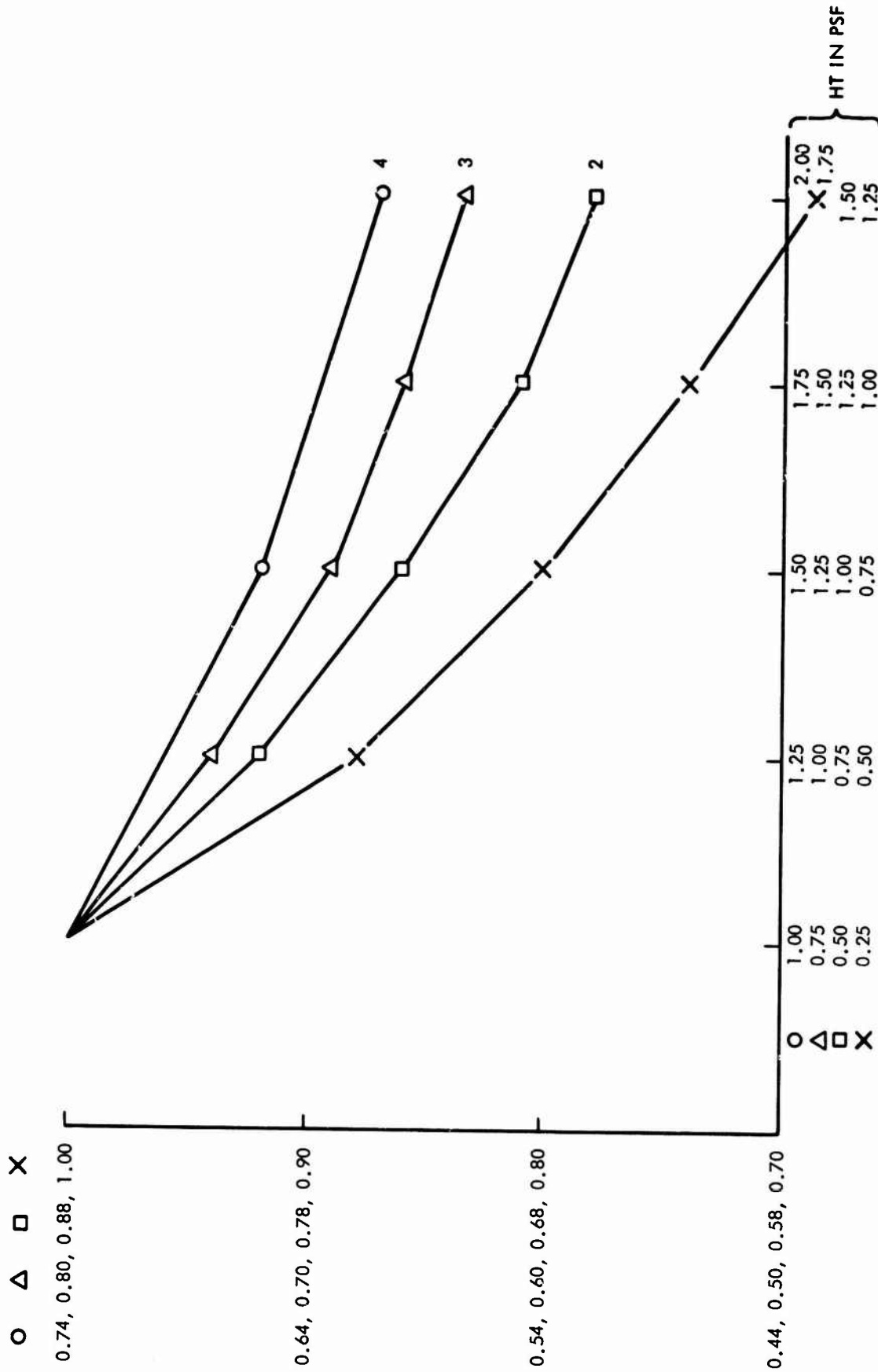
FIG. 4 Various segments of the curve of theoretical exposure vs matter thickness (height) above ground, plotted so that all curves intersect in a single point, that for which L (3ft) = 1.00. The data of FIG. 3 lie along curve 2, indicating a ground roughness, Δh = 3 ft. (conversion formula: 0.25 psf = 3 ft).

HT IN PSF

4 3 2

2.00 1.75 1.50 1.25

1.75 1.50 1.25 1.00

1.50 1.25 1.00 0.75

1.25 1.00 0.75 0.50

1.00 0.75 0.50 0.25

○ △ □ ✕

0.74, 0.80, 0.88, 1.00

0.64, 0.70, 0.78, 0.90

0.54, 0.60, 0.68, 0.80

0.44, 0.50, 0.58, 0.70

3. PLANE SLAB HAVING ARBITRARY ORIENTATION

A. Geometrical Preliminaries

We choose cartesian coordinates (x_o, y_o) in the plane of the slab, Σ, with the $\hat{x}_o$ - axis* horizontal and the $\hat{y}_o$ - axis forming an angle α with the vertical, where $\alpha = +\frac{\Gamma}{2}$ for the floor (Figure 5). The origin of coordinates, O, is the intersection of the perpendicular to the $x_o y_o$ - plane from the detector position $D = D(0,0,z_1)$ where $z_1 > 0$ is the distance from slab to detector; the detector is positioned at height h above the horizontal plane of the ground. In addition we employ spherical coordinates, with origin at D and polar axis pointing down. The co-latitude angle of the point $P(x_o, y_o, 0)$ at which the incident γ-ray passes through Σ is θ, by the definition given above eq. (2.1). The unit vector which points from D to P is $\hat{n}$ and the azimuth of $\hat{n}$ in the plane parallel to the ground (through D) measured from $+\hat{x}$, counter-clockwise from above, is φ, the second polar variable of the point** P. In Figure 5 we have included also an auxiliary (primed) set of cartesian axes, having the same origin O and $\hat{y}_o'$ - axis pointing vertically upwards. From

$$\hat{n} = -\hat{y}_o' \cos\theta + (\hat{x}_o' \cos\varphi - \hat{z}_o' \sin\varphi)\sin\theta \tag{3.1}$$

$$\hat{x}_o' = \hat{x}_o \tag{3.2a}$$

$$\hat{y}_o' = -\hat{z}_o \sin\alpha + \hat{y}_o \cos\alpha, \tag{3.2b}$$

$$\hat{z}_o' = \hat{z}_o \cos\alpha + \hat{y}_o \sin\alpha \tag{3.2c}$$

we have

$$\hat{n} = \hat{x}_o \cos\varphi \sin\theta - \hat{y}_o (\cos\varphi \cos\alpha + \sin\theta \sin\alpha \sin\varphi)$$
$$+ \hat{z}_o (\cos\varphi \sin\alpha - \sin\theta \cos\alpha \sin\varphi). \tag{3.3}$$

---

*Generally, we use the carat to denote a direction (unit) vector
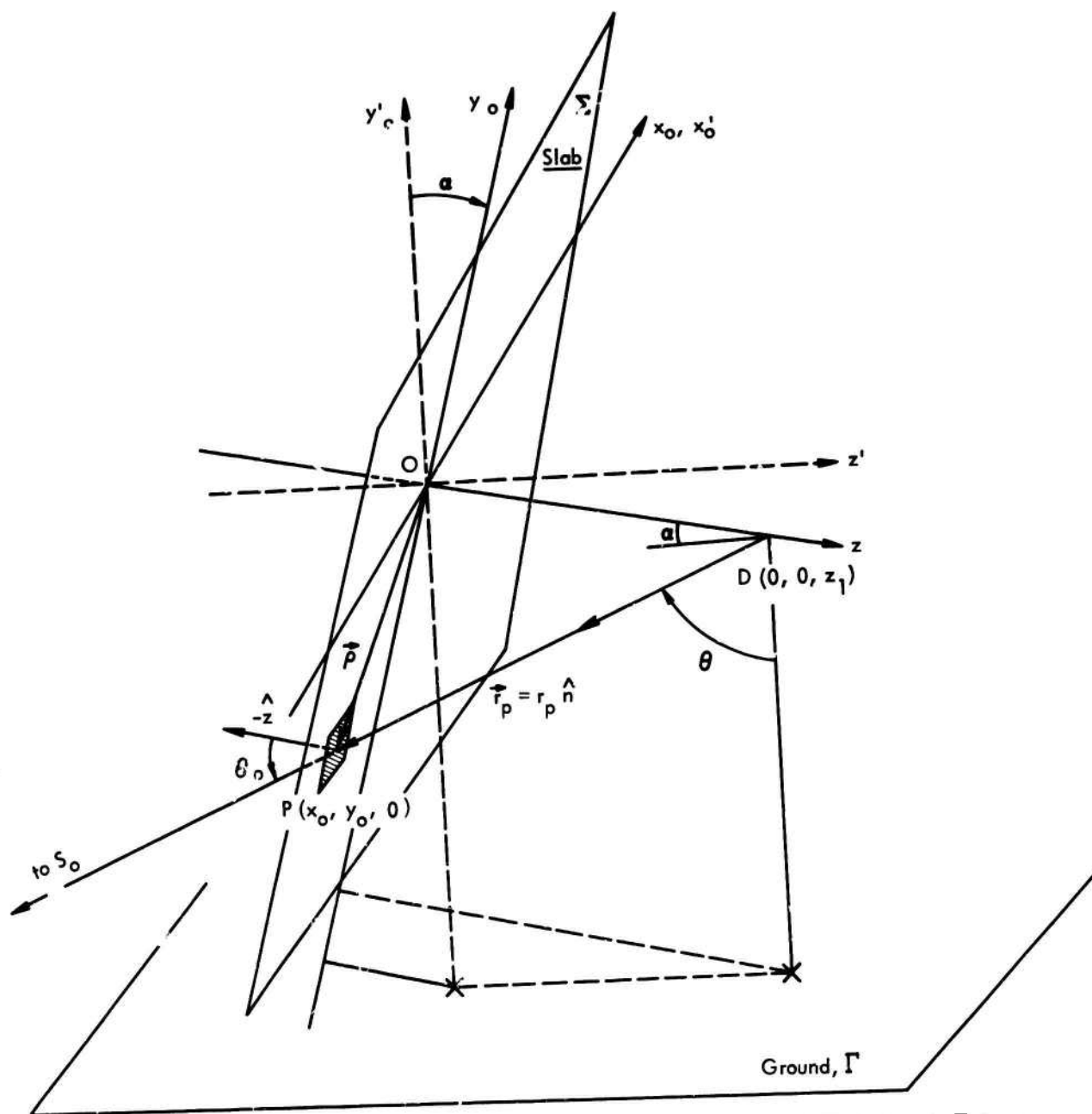

**The spherical coordinate system is left-handed.

FIG. 5 Geometry of slab (Σ) orientation, detector (D) position, γ-ray path (PD) through Σ from the ground, Γ. For the configuration shown, $\alpha > 0$.

We denote the vector $\vec{OP}$ by $\vec{\rho}_P$ and $\vec{PD}$ by $\vec{r}_P$ so that

$$\vec{r}_P = r_P \hat{n} = \vec{\rho}_P - z_1 \hat{z}_o \tag{3.4}$$

and

$$\vec{\rho}_P = x_o \hat{x}_o + y_o \hat{y}_o \tag{3.5}$$

$$r_P = (x_o^2 + y_o^2 + z_1^2)^{\frac{1}{2}}, \tag{3.6}$$

whence, using eq. (3.4), we find

$$x = x(x_o, y_o) = \cos\theta = -r_P^{-1} y_o \cos\alpha - r_P^{-1} z_1 \sin\alpha \tag{3.7}$$

$$\tan\varphi = -x_o^{-1} y_o \sin\alpha + x_o^{-1} z_1 \cos\alpha, \tag{3.8}$$

and

$$\frac{\partial(x,\varphi)}{\partial(x_o, y_o)} = - z_1 r_P^{-3}, \tag{3.9}$$

so that integrals of the type appearing in eq. (2.3) can be performed on the plane of the slab,

$$\frac{1}{2\pi} \int d\Omega g_\Sigma(\Omega) \cdots = \frac{1}{2\pi} \int_{x_1}^{x_2} \int_{y_1}^{y_2} dx_o dy_o \cdot \frac{z_1}{r_P^3} \cdots, \tag{3.10}$$

where the "left" and "right" edges of Σ are located at $x_o = x_1$ and $x_o = x_2$, respectively, and the "lower" and "upper" edges by $y_o = y_1$ and $y_o = y_2$, respectively. If we let

$$\xi = x_o z_1^{-1}, \quad \eta = y_o z_1^{-1}, \tag{3.11}$$

then for (3.10) we may write

$$\frac{1}{2\pi} \int d\Omega g_\Sigma(\Omega) \cdots = \frac{1}{2\pi} \int_{\xi_1}^{\xi_2} d\xi \int_{\eta_1}^{\eta_2} d\eta \, (\xi^2 + \eta^2 + 1)^{-3/2} \cdots, \tag{3.12}$$

where $\xi_i = x_i z_i^{-1}$ and $\eta_i = y_i z_i^{-1}$, $i = 1, 2$.

We also need to express θ_o in terms of the cartesian variables; from

$$\cos\theta_o \equiv \hat{n} \cdot (-\hat{z}_o), \tag{3.13}$$

with eq. (3.3),

$$\cos\theta_o = - \cos\theta \sin\alpha + \sin\theta \cos\alpha \sin\varphi, \tag{3.14}$$

15

whence with the aid of eqs. (3.7) and (3.8)

$$\cos \theta_o = (\xi^2 + \eta^2 + 1)^{-\frac{1}{2}}, \tag{3.15}$$

which also can be seen by inspection (Figure 3).

B. Basic Geometrical Approximation Scheme

There are two classes of slab orientation we need to consider: (i) $|\alpha|$ well away from $\frac{\pi}{2}$, as in the case that Σ is a wall; and (ii) $\alpha = \pm \frac{\pi}{2}$, where Σ is a ceiling or a floor. For the latter we adopt the approximation scheme described in Reference 2, which replaces Σ by another slab, Σ_o, formed of suitable combinations of circles and annular sectors -- so we discuss only case (i) here.

The integrand of eq. (2.3) is peaked at $x = \varkappa$ owing to the form of $l(h,x)$. The intersection of the plane of Σ and the cone of constant x with vertex at the detector is a conic section, and $l(h,x)$ is constant along this curve. We exploit this fact by transforming integrations over Σ to elliptical coordinates, u, v, in the plane of Σ, so chosen that the curve $x = \varkappa$, which (normally) is a hyperbola, coincides with one of the curves of constant v: $v = v_1$. From eq. (3.7)

$$x = -(\xi^2 + \eta^2 + 1)^{-\frac{1}{2}} (\eta \cos \alpha + \sin \alpha), \tag{3.16}$$

so the hyperbola, which results when $\cos^2 \alpha > x^2$ is

$$a^{-2}(\eta + b)^2 - c^{-2} \xi^2 = 1 \tag{3.17}$$

where, for $x = \varkappa$

$$b = \sin \alpha \cos \alpha (\cos^2 \alpha - \varkappa^2)^{-1} \tag{3.18}$$

$$\doteq \tan \alpha + 0(\varkappa^2), \quad \varkappa << 1, \tag{3.18'}$$

$$a^2 = \varkappa^2 (1-\varkappa^2)(\cos^2 \alpha - \varkappa^2)^{-2} \tag{3.19a}$$

$$c^2 = (1 - \varkappa^2)(\cos^2 \alpha - \varkappa^2)^{-1}. \tag{3.19b}$$

The angle $|\psi|$ formed by the $\hat{x}_o$ - axis and the asymptotes to (3.17) is given by

$$\tan |\Psi| = a/c = \varkappa (\cos^2 \alpha - \varkappa^2)^{-\frac{1}{2}} \tag{3.20}$$

$$|\psi| \doteq \varkappa + 0(\varkappa^3), \quad \varkappa << 1. \tag{3.20'}$$

Half the distance between the foci, P_1 and P_2, is

$$D = z_1(a^2 + c^2)^{\frac{1}{2}}$$

$$= z_1(1 - \varkappa^2)^{\frac{1}{2}} \cos \alpha (\cos^2\alpha - \varkappa^2) \tag{3.21}$$

$$\doteq z_1 \sec \alpha + O(\varkappa^2), \quad \varkappa \ll 1. \tag{3.21'}$$

We introduce the elliptical coordinates as follows. We let r_1 and r_2 be distances of $P(x_o, y_o)$ from $P_1(0, -bz_1-D)$ and $P_2(0, -bz_1+D)$ and define

$$u = (2D)^{-1}(r_1+r_2), \quad v = (2D)^{-1}(r_1-r_2). \tag{3.22}$$

We need the following relations, which follow from the above:

$$\eta = Dz_1^{-1} uv - b \tag{3.23}$$

$$\sec \theta_o = (\xi^2 + \eta^2 + 1)^{\frac{1}{2}}$$

$$= Dz_1^{-1}[u^2 - 2v_o vu + v^2 - v_1^2(1-v_o^2)]^{\frac{1}{2}}, \tag{3.24}$$

where

$$v_o = \sin \alpha \quad \text{and} \quad v_1 = -\varkappa \sec \alpha, \tag{3.25}$$

the latter being the value of v for which $x = \varkappa$ holds; also

$$x = - \cos \alpha (uv - v_o v_1^2)[u^2 - 2v_o uv + v^2 - v_1^2(1 - v_1^2)]^{-\frac{1}{2}}, \tag{3.26}$$

$$\frac{\partial(\xi, \eta)}{\partial(u, v)} = \left(\frac{D}{z_1}\right)^2 (u^2 - v^2)[(u^2 - 1)(1 - v^2)]^{-\frac{1}{2}}. \tag{3.27}$$

For the approximation to small $\varkappa$, we drop the v_1^2 terms in eqs. (3.24) and (3.26),

$$\sec \theta_o \doteq \sec \theta_o (u^2 - 2v_o uv + v^2)^{\frac{1}{2}} \tag{3.24^1}$$

$$x \doteq - uv \cos \alpha (u^2 - 2v_o uv + v^2)^{-\frac{1}{2}} \tag{3.26^1}$$

For eq. (3.10) we have

$$\frac{1}{2\pi} \int d\Omega g_\Sigma(\Omega) \cdots \doteq \frac{\cos \alpha}{2\pi} \iint_\Sigma dudv (u^2 - v^2)[(u^2 - 1)(1 - v^2)]^{-\frac{1}{2}}$$

$$\times (u^2 - 2v_o uv + v^2)^{-3/2} \cdots. \tag{3.28}$$

where the $\cos \alpha$ in front comes from the scale factor $(D/z_1)^2 \cdot (D/z_1)^{-3}$ (cf. eqs. (3.24) and (3.27)).

17

The integrand of E_Σ, in eq. (2.3), is proportional to

$$\ell(h,x) \; \exp \; (-a_\Sigma \sec \beta \theta_o)$$

where

$$a_\Sigma = \mu_\Sigma t_\Sigma. \tag{3.29}$$

We **approximate this by taking** $\beta \doteq 1$:

$$\sec \beta \theta_o = \sec \theta_o - (1-\beta)\theta_o \sec \theta_o \tan \theta_o + - - -,$$

so

$$e^{-a_\Sigma \sec \beta \theta_o} = e^{-a_\Sigma \sec \theta_o}(1 + (1 - \beta)\theta_o \sec \theta_o \tan \theta_o + - - -) \tag{3.30}$$

$$\doteq e^{-a_\Sigma \sec \theta_o} \tag{3.30'}$$

The approximation to (3.30$'$) is reasonable if $|\alpha|$ is not too large, so that θ_o is relatively small in regions where $\ell(h,x)$ peaks. For $x>0$ we have

$$\ell(h,x) e^{a_\Sigma \sec \theta_o} = cx^{-1}\exp[-x^{-1}(\varkappa - a_\Sigma uv)], \; x>0 , \tag{3.31}$$

by eqs. (2.20), (3.24$'$), (3.26$'$), and for $x<0$,

$$\ell(h,x) = [c_1 + c_2(x + 1)^2] \exp (x^{-1}a_\Sigma uv), \; x<0. \tag{3.32}$$

The main observation now is that $x(u,v)$ is only weakly u - dependent in regions where $\ell(h,x)$ is big. To see this we evaluate $(\partial x(u,v)/\partial u)_v$,

$$\left(\frac{\partial x}{\partial u}\right)_v \doteq - \cos \alpha (u^2 - 2 \sin \alpha \cdot u v + v^2)^{-3/2}$$

$$\times (v^3 - \sin \alpha \cdot uv^2), \tag{3.33}$$

where the spirit of the approximation is the same as that used to get eqs. (3.24$'$) and (3.26$'$); the exact expression for $(\partial x/\partial u)_v$ vanishes identically at $v = v_1 = -\varkappa \sec \alpha$, where $x = \varkappa$, and for $v = 0(\varkappa)$, $(\partial x/\partial u)_v = 0(\varkappa^2)$. For $\alpha = 0$, we have

$$\left| (\partial x/\partial u)_v \right| \doteq \left[\left(\frac{u}{v}\right)^2 + 1 \right]^{-3/2}$$

which, even for $|v| = .4$, satisfies $|\partial x/\partial u)v| \simeq 5\%$ since $u \geq 1$ by eq. (3.22); and $x(1,.4) = .36 \sim 20\varkappa$, for $\varkappa = .018$, a value larger than is needed for our purposes. So in (3.31) and (3.32) we replace $x(u,v)$ with $x(1,v)$, approximating the curves of constant θ, on Σ, by curves of constant v, for values of v well away from v_1, where this result is exact. The results are worked out in Section 4.

18

Finally we introduce a certain geometrical approximation $\sum_o$, to the shape $\sum$, which does not enjoy complete generality but which does cover a reasonably wide range of circumstances, those of the present application, in particular. We simply insert constant, suitable chosen limits u_1, u_2, and v_1, v_2 into the integral on the right side of (3.28) so that

$$\frac{1}{2\pi} \int d\Omega g_{\sum}(\Omega) \cdots \doteq \frac{1}{2\pi} \int d\Omega g_{\sum_o}(\Omega) \cdots$$

$$\doteq \frac{\cos\alpha}{2\pi} \sum_{i=1}^{2} \int_1^{u_1} du \int_{v_1}^{v_2} dv (u^2 - v^2)[(u^2-1)(1-v^2)]^{-\frac{1}{2}}$$

$$\times (u^2 - 2\sin\alpha \cdot uv + v^2)^{-3/2} \cdots, \quad (3.34)$$

where the sum arises from the fact that the coordinates u,v only cover half the $x_o y_o$ - plane, e.g. the $x_o \geq 0$ half, and we have assumed that $x_1 < 0 < x_2$. If $0 \notin (x_1, x_2)$, the sum in (3.34) is replaced by a difference; i.e., a single term, written as $\int_{u_1}^{u_2} du \int_{v_1}^{v_2} dv \ldots$ suffices.

For all of the circumstances of interest to us here we may choose u_i to correspond to the ellipse passing through the point $(x_o, y_o) = (x_i, 0)$; this gives

$$u_i \equiv \sec\Theta_i = (x_i^2 + D^2)^{\frac{1}{2}}/D \doteq (1 + \xi_i^2 \cos^2\alpha)^{\frac{1}{2}}. \quad (3.35)$$

The main fact making this choice possible is that in all cases here the upper and lower edges of $\sum$, at $y_o = y_1$ and y_2, lie between the foci of the coordinate system, at $P_1 = P_1(0, -bz_1 - D)$ and $P_2 = P_2(0, -bz_1 + D)$. In almost all of these the analogous choice

for v_i is a good enough approximation*, that v_i correspond to the hyperbola passing through $(x_o, y_o) = (0, y_i)$. Then, by the second of eqs. (3.22), and eqs. (3.18') and (3.21'),

$$v_i = (y_i + bz_1)D^{-1} \doteq \eta_i \cos\alpha + \sin\alpha. \quad (3.36)$$

---

* The exception is dealt with in Section 5.

Figures 6 and 7 show examples for two of the surfaces from the M113,
illustrating all of the above features. The choice of $\sum_o$ defined
by eqs. (3.35) and (3.36) we refer to as the <u>centered</u>
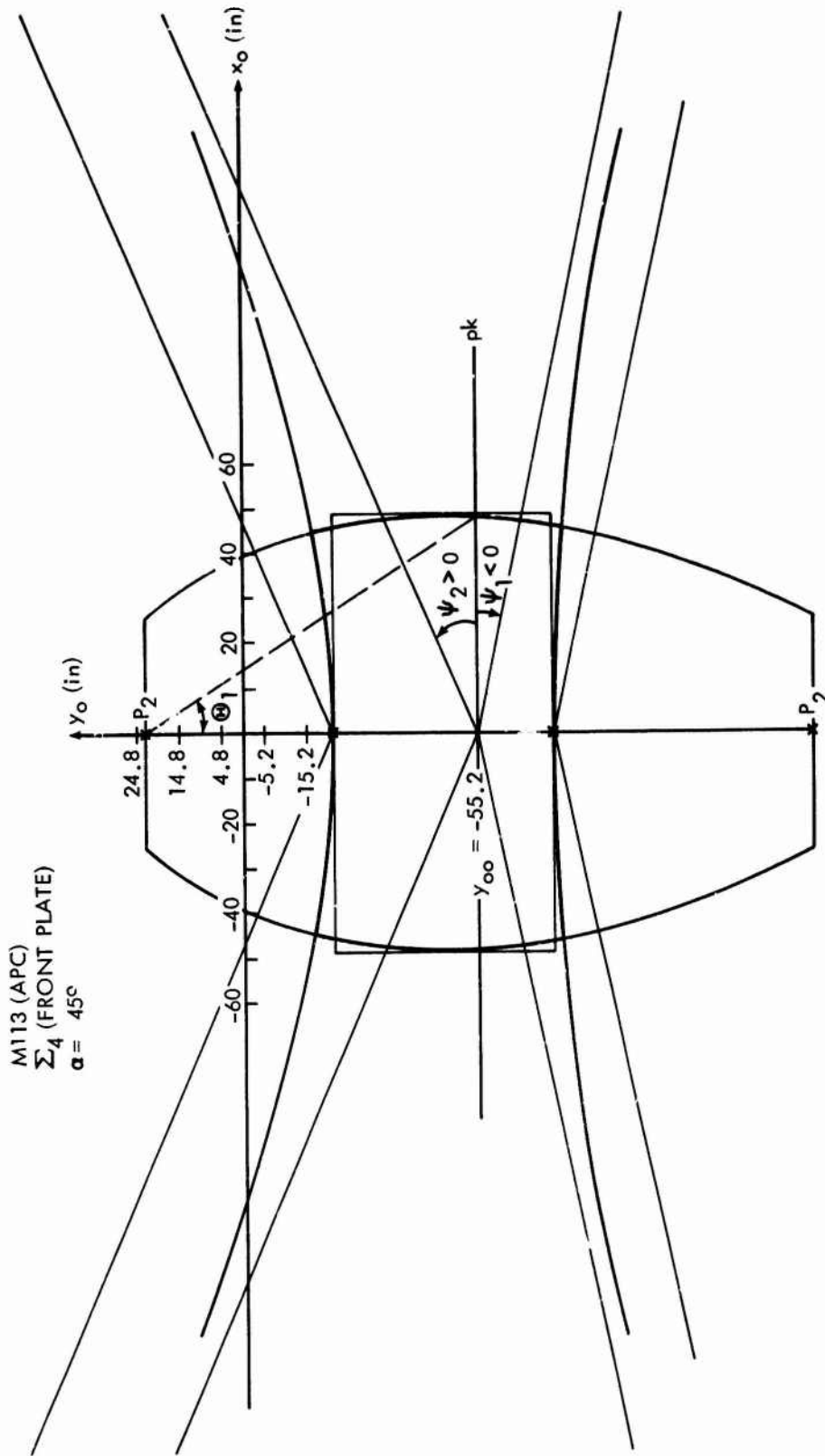<u>approximation</u>.

FIG. 6 Centered approximation to the M113 surface Σ_4. P and P_2 are the foci of the elliptical coordinate system and the $\hat{x}_o$ - and $\hat{y}_o$- axes are those of FIG. 5. The curves of constant u are ellipses and the curves of constant v are hyperbolas. The point $x_o = 0$, $y_o = y_{oo}$ is the mid-point of $P_1 P_2$. The ellipse $u = u_1$ is tangent to the side edges of Σ_4, the hyperbola $v = v_1$ is tangent to the bottom edge ($y_o = y_1$), and the hyperbola $v = v_2$ is tangent to the top edge ($y_o = y_2$).

M113 (APC)
Σ_5 (LOWER FRONT PLATE)
$a = -30°$

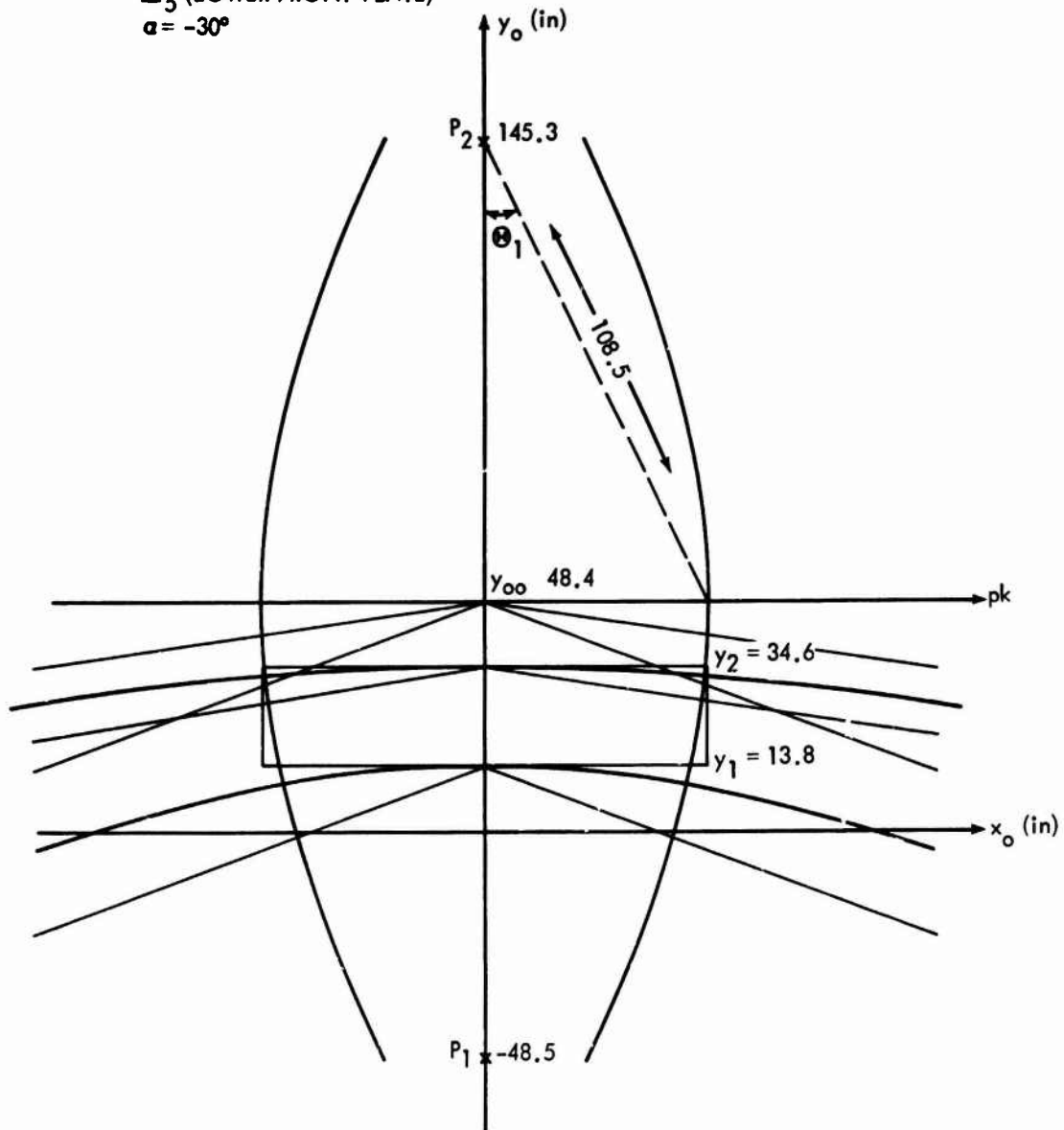
FIG. 7 Same as FIG. 6, but Σ_5 rather than Σ_4. Here the ellipse $u = u_1$ is tangent to the extension of the side edges since the midpoint of $P_1 P_2$ lies above the rectangle $(y_{aa} > y_1$ and $y_{ao} > y_2)$.

22

4. EXPRESSIONS FOR THE E_Σ's, AND $\mathcal{R}$.

    A. **Class i. Wall Slabs ($|\alpha|$ Away From $\pi/2$).**

    It suffices to treat the case $x_1 = -x_2$ so that $u_1 = u_2$; this is the symmetrical case. For the asymmetrical case, $u_1 \neq u_2$, the right side of (3.34) is the average of the two symmetrical results for u_1 and u_2.

    We evaluate (3.34) first with the "$\cdots$" replaced by 1; the resulting expression gives the solid angle factor for Σ_o at the detector position, namely $(2\pi)^{-1}$ times the solid angle substended at $D(0,0,z_1)$ by Σ_o.

$$\omega_{\Sigma_o} \doteq \frac{\cos \alpha}{\pi} \int_1^{u_2} du \int_{v_1}^{v_2} dv (u^2 - v^2)[(u^2 - 1)(1 - v^2)]^{-\frac{1}{2}}$$

$$\times (u^2 - 2 \sin \alpha . uv + v^2)^{-3/2} . \tag{4.1}$$

Using

$$\rho^{-3} = u^{-2} v^{-1} \sum_{m=1}^{\infty} P_n' (\sin \alpha) \left(\frac{v}{u}\right)^n, \qquad |v/u| < 1, \tag{4.2}$$

where

$$\rho = \rho(\sin \alpha) = (u^2 - 2 \sin \alpha \cdot uv + v^2)^{\frac{1}{2}} \tag{4.3}$$

and P_n is the Legendre polynomial of order n, the prime denoting differentiation by the argument, we have

$$\omega_{\Sigma_o} \doteq \frac{\cos \alpha}{\pi} \int_1^{u_2} du(u^2 - 1)^{-\frac{1}{2}} \int_{v_1}^{v_2} dv(1-v^2)^{-\frac{1}{2}}[1-(v/u)^2]v^{-1}$$

$$\cdot \sum_{n=1}^{\infty} P_n^1 (\sin \alpha)(v/u)^n . \tag{4.4}$$

We define

$$I_n = \int_1^{u_2} du\, u^{-n}(u^2 - 1)^{-\frac{1}{2}} = \int_0^{\Theta_2} d\theta \, \cos^{n-1}\theta \tag{4.5a}$$

$$J_n = \int_{v_1}^{v_2} dv\, v^{n-1}(1 - v^2)^{-\frac{1}{2}} = \int_{\Psi_1}^{\Psi_2} d\Psi \, \sin^{-1}\Psi, \tag{4.5b}$$

where

$$v_i = \sin \Psi_i, \qquad i = 1,2, \tag{4.6}$$

with Θ_2 given by eq. (3.35), and interchange orders of integration

23

and summation to get

$$\omega_{\Sigma_O} \doteq \frac{\cos \alpha}{\pi} \sum_{n=1}^{\infty} P_n' (\sin \alpha)(I_n J_n - I_{n+2} J_{n+2}) \qquad (4.7)$$

$$\doteq \frac{\cos \alpha}{\pi} \sum_{n=0}^{\infty} (2n + 1) P_n (\sin \alpha) I_{n+1} J_{n+1}, \qquad (4.8)$$

in which we have used the identity $P_{k+1}'(x) - P_{k-1}'(x) = (2k+1) P_k(x)$.
The key feature of the expansion, eq. (4.8), is that successive
terms diminish rapidly owing to eq. (4.5b) : the expansion parameters
are the Ψ_i because the lowest order term of the Taylor series for
$J_n(\Psi_1, \Psi_2)$ is $n^{-1}(\Psi_2^n - \Psi_1^n)$. From eqs. (4.5), (4.6) and (4.8) we have

$$\omega_{\Sigma_O} \doteq \frac{\cos \alpha}{\pi} \left[\Theta_2 \Psi + \frac{3}{2} \sin \alpha \sin \Theta_2 \cdot \Psi^2 \right.$$

$$\left. - \frac{5}{12}(3 \sin^2 \alpha - 1)(\Theta_2 + \sin \Theta_2 \cos \Theta_2) \cdot \Psi^3 + \cdots \right]_{\Psi_1}^{\Psi_2}. \qquad (4.9)$$

The solid angle factor for Σ can be computed exactly for
comparison; it is the difference of the solid angle factors for the
rectangles Σ_2 and Σ_1, having common upper edge at $y_o = 0$ and lower
edges at (respectively) $y_o = y_2$ and $y_o = y_1$ (cf Figure 6),

$$\omega_\Sigma = \omega_{\Sigma_2} - \omega_{\Sigma_1}, \qquad (4.10)$$

where, from eq. (3.12)

$$\omega_{\Sigma_i} = \frac{1}{\pi} \int_0^{\xi_2} d\xi \int_0^{\eta_i} d\eta \ (\xi^2 + \eta^2 + 1)^{-3/2} \qquad (4.11)$$

$$= \frac{1}{\pi} \tan^{-1}[\eta_{1,2} \xi_2 (1 + \eta_i^2 + \xi_2^2)^{-\frac{1}{2}}] \qquad (4.12)$$

For the case shown in Figure 6, $z_1 = 55.2"$, $y_1 = -72.1"$,
$y_2 = -20.8"$, and $x_2 = 49.1"$, which yields

$$\omega_\Sigma = .1016$$

The parameters of Σ_O in the centered approximation are obtained
from eqs. (3.21'), (3.35), and (3.36) with $\alpha = 45°$; we find $D = 78"$,
$\Theta_2 = .5620$, $\Psi_1 = -.2181$, and $\Psi_2 = .4556$, so that eq. (4.9) gives

$$\omega_{\Sigma_0} \doteq .0852 + .0203 - .0050 \doteq .1005,$$

which agrees with the exact result for ω_Σ to less than 2%.

We apply to E_Σ the methods used to obtain eqs. (4.8) and (4.9). With the help of eqs. (3.26'), (3.31) and (3.32) the analogue of eq. (4.4) is

$$E_{\Sigma_0} \doteq \frac{\cos \alpha}{\pi} \int_1^{u_2} du (u^2-1)^{-\frac{1}{2}} \int_{v_1}^{v_2} dv (1-v^2)^{-\frac{1}{2}} [1-(v/u)^2] v^{-1}$$

$$[\theta(-v) c x^{-1} \exp(-\varkappa x^{-1}) + \theta(v)(c_1 + c_2 (x+1)^2]$$

$$\cdot \exp(-A_\Sigma u) \sum_{n=1}^{\infty} P_n' (\sin \alpha)(v/u)^n, \qquad (4.13)$$

where $\theta(v)$ denotes the unit step function, which vanishes for $v<0$, and

$$A_\Sigma \equiv -a_\Sigma v x^{-1} \qquad (4.14)$$

In the approximation discussed near the end of Section 3, $x(u,v) \approx x(1,v)$, so that also $A_\Sigma (u,v) \approx A_\Sigma (1,v)$. In parallel with eqs. (4.5) we define

$$I_n(v) = \int_1^{u_2} du\, u^{-n} (u^2-1)^{-\frac{1}{2}} \exp(-A_\Sigma(1,v)u) \qquad (4.15a)$$

$$J_n = \int_{v_1}^{v_2} dv\, v^{n-1} (1-v^2)^{-\frac{1}{2}} \ell_1(v), \qquad (4.15b)$$

where $\ell_1(v)$ stands for the square bracketed expression in (4.13) with $x = x(1,v)$. We write $I_n(v)$ as a Taylor series in v,

$$I_n(v) = \sum_{m=0}^{\infty} \frac{v^m}{m!} I_n^{(m)}(0), \qquad (4.16)$$

substitute this with eqs. (4.15) into (4.13) and rearrange the summations to get the analogue of eq. (4.8),

$$E_{\Sigma_0} \doteq \frac{\cos \alpha}{\pi} \sum_{r=0}^{\infty} J_{r+1} \sum_{m=0}^{r} (2n+1) P_n (\sin \alpha) \frac{I_{n+1}^{(r-n)}(0)}{(r-n)!} \qquad (4.17)$$

Keeping only the first two terms, we obtain an approximation whose spirit is only a little rougher than that of eq (4.9),

$$E_\Sigma \approx \frac{\cos \alpha}{\pi} \left[I_0^{(0)}(0) J_1 + (I_1^{(1)}(0) + 3 \sin \alpha\, I_2^{(0)}(0)) J_2 \right]. \qquad (4.18)$$

NOLTR 73-137

The analogous approximation to ω_Σ for the example of Figure 6, just discussed, agrees with ω_Σ to a few percent (1.4%). We note that

$$I_n^{(0)}(0) = I_n(0) \tag{4.19a}$$

$$I_n^{(1)}(0) = -\frac{dA_\Sigma}{dv}\bigg|_0 \cdot I_{n-1}(0)$$

$$= a_\Sigma \tan \alpha \cdot I_{n-1}(0), \tag{4.19b}$$

so eq. (4.18) may be rewritten as

$$E_{\Sigma_0} \approx \frac{\cos \alpha}{\pi}\left[I_1(0)J_1 + (3 \sin \alpha \cdot I_2(0) + a_\Sigma \tan \alpha \cdot I_0(0))J_2\right] \tag{4.20}$$

If $\alpha = 0$, this has an especially simple form;

$$E_{\Sigma_0} \approx \frac{1}{\pi} I_1(0)J_1, \quad \alpha = 0. \tag{4.21}$$

To complete the scheme we develope expressions for J_1 and J_2 for use in eq. (4.20). The $I_n(0)$ present no difficulty because $I_1(0)$ is the Sievert integral; changing variables in eq. (4.15a),

$$I_1(0) = \int_0^{\Theta_2} d\theta \exp(-A_\Sigma(1,0)\sec \theta) = S(A_\Sigma(1,0),\Theta_2), \tag{4.22a}$$

which is tabulated;[5] we note from eqs. (3.26') and (4.4) that

$$A_\Sigma(1,0) = a_\Sigma \sec \alpha. \tag{4.22b}$$

$I_0(0)$ is found by differentiating (4.22a),

$$-\frac{\partial s(A,\theta_2)}{\partial A} = \int_0^{\Theta_2} d\theta \sec \theta \exp(-A \sec \theta)$$

$$= \int_1^{u_2} du(u^2-1)^{-\frac{1}{2}} \exp(-Au), \tag{4.23}$$

and this can be determined from the tabulation of S to adequate accuracy by numerical differentiation. Finally by examining the expansions of $I_n(0)$ in powers of Θ_2 for $n = 0$ and $n = 2$ we can produce the approximation,

$$I_2(0) \approx -I_0(0) + 2 I_1(0) + \frac{1}{20}\Theta_2^5 \exp(-a_\Sigma \sec \alpha). \tag{4.24}$$

The coefficients of the expansions of both sides agree up to and including the Θ_2^6 - term.

26

Turning to J_1 and J_2, we treat the direct and skyshine parts separately, writing

$$J_n = J_n^{(d)} + J_n^{(s)} \qquad (4.25)$$

where the integration in $J_n^{(d)}$ extends over the range of values of v for which $x>0$, while in $J_n^{(s)}$, $x<0$ always holds. In the integrand of the direct contribution we extract a peak factor,

$$-(v \cos \alpha)^{-1} \exp [+ \varkappa (v \cos \alpha)^{-1}],$$

and expand the rest in powers of v. Integrating term by term produces a series of exponential integrals, $E_k(\zeta_i)$, having small arguments when $\varkappa \ll 1$

$$E_k(\zeta_i) = \int_{\zeta_i}^{\infty} d\zeta \, \zeta^{-k} e^{-\zeta}$$

where

$$\zeta_i = \varkappa \sec \alpha \cdot (-v_i)^{-1}, \qquad (4.26)$$

in which v_i means v_1 or v_2. Using

$$E_2(\zeta_i) = \zeta_i^{-1} \exp(-\zeta_i) - E_1(\zeta_i),$$

we find, for $v_1 < 0 < v_2$,

$$J_1^{(d)} \approx c \sec \alpha \left\{ E_1(\zeta_1) - \left[e^{-\zeta} \sin \alpha (1 - \varkappa (\tan \alpha + \tfrac{1}{2} \cot \alpha)) v \right]_{v_1}^{0} \right\}, \qquad (4.27a)$$

and for $v_1 < v_2 < 0$,

$$J_1^{(d)} \approx c \sec \alpha \left\{ \left[E_1(\zeta) - e^{-\zeta} \sin \alpha (1 - \varkappa (\tan \alpha + \tfrac{1}{2} \cot \alpha)) v \right]_{v_1}^{v_2} \right\}; \qquad (4.27b)$$

also, for $v_1 < 0 < v_2$,

$$J_2^{(d)} \approx c \sec \alpha \left\{ -\varkappa \sec \alpha \, E_1(\zeta) + \left[e^{-\zeta} (1 - \varkappa \tan \alpha) v \right]_{v_1}^{0} \right\} \qquad (4.28a)$$

and, for $v_1 < v_2 < 0$,

$$J_2^{(d)} \approx c \sec \alpha \left\{ \left[-\varkappa \sec \alpha \, E_1(\zeta_1) + e^{-\zeta} (1 - \varkappa \tan \alpha) v \right]_{v_1}^{v_2} \right\}. \qquad (4.28b)$$

For the skyshine part we expand the integral and integrate: for $v_1 < 0 < v_2$,

$$J_1^{(s)} \approx (c_1 + c_2) v \left.\right|_0^{v_2} , \quad J_2^{(s)} \approx 0, \qquad\qquad (4.29)$$

and for $v_1 < v_2 < 0$,

$$J_1^{(s)} = 0, \quad J_2^{(s)} = 0. \qquad\qquad (4.30)$$

In eqs. (4.27) through (4.29) we have dropped terms of order κ^2 and, in comparison with $E_1(\zeta_i)$, we have neglected terms of order v_1^2 and v_2^2.

B. Class ii. Floor and Ceiling Slabs $(\alpha = \pm \frac{\pi}{2})$.

The method we use in these cases is described in Reference 2, so we mainly just give the results of using the source indicated in eq. (2.20).

Floor $(\alpha = -\pi/2$.

We suppose the detector position to be above the center of a rectangular floor Σ. Σ_0 is a shape compounded of a centered circle of radius r, and two equal, symmetrically placed, annular sectors having radii r_1 and $r_2 > r_1$, concentric and with angle ψ_0. r_1 is determined by the requirement that the solid angle factor subtended at D by the circle equal that of a concentric square having side equal to the width of Σ, which is ω_Σ'; r_2 is determined the same way, with the side of the square equal to the length of Σ, the solid angle factor being ω_Σ''; and ψ_0 is fixed by requiring $\omega_{\Sigma_0} = \omega_\Sigma$.

Ceiling $(\alpha = +\pi/2)$.

Since the skyshine is only about 10% of the total, a coarser approximation will do. We let Σ_0 be a circle whose radius, r_1, is so chosen that $\omega_\Sigma = \omega_{\Sigma_0}$. This may be regarded as a special case of the surface used above to represent the floor, one in which $r_2 = r_1$.

If Σ already is a square, $\omega_\Sigma' = \omega_\Sigma'' = \omega_\Sigma$ and $r_2 = r_1$ automatically hold, and Σ_0 becomes a circle.

With

$$r_i \equiv z_1 \lambda_i \equiv z_1 \tan \theta_i, \quad i = 1, 2, \tag{4.31}$$

we have

$$\sec \theta_i = (1 - \omega_\Sigma(i))^{-1}, \quad i = 1, 2, \tag{4.32}$$

$$\varphi_0 / \pi = (\omega_{\Sigma''} - \omega_{\Sigma'})^{-1} (\omega_\Sigma - \omega_{\Sigma'}). \tag{4.33}$$

Expressions for the $\omega_{\Sigma(i)}$ may be produced easily from eq. (4.12). From the form (see eqs. (2.3), (2.20), (3.14), (3.15), (3.12)),

$$E_\Sigma = \frac{1}{2\pi} \int_{\xi_1}^{\xi_2} d\xi \int_{\eta_1}^{\eta_2} d\eta (\xi^2 + \eta^2 + 1)^{-1} c \exp\left[-A(\xi^2 + \eta^2 + 1)^{\frac{1}{2}}\right], \quad \alpha = -\frac{\pi}{2}, \tag{4.34}$$

where

$$A \equiv a_\Sigma + \varkappa, \tag{4.35}$$

we convert to integration over $\sum_0$, which gives

$$E_{\Sigma_0} = c \int_0^{\lambda_1} d\lambda \, \lambda (\lambda^2 + 1)^{-1} \exp\left[-A(\lambda^2 + 1)^{\frac{1}{2}}\right] + (\varphi_0/\pi) c \int_{\lambda_1}^{\lambda_2} d\lambda \, \lambda (\lambda^2 + 1)^{-\frac{1}{2}} \exp(-A(\lambda^2 + 1)^{\frac{1}{2}}) \tag{4.36}$$

$$= E_1(A) - [1 - (\varphi_0/\pi)] E_1(A \sec \theta_1) - (\varphi_1/\pi) E_1(A \sec \theta_2); \tag{4.37}$$

and from the form,

$$E_\Sigma = \frac{1}{2\pi} \int_{\xi_1}^{\xi_2} d\xi \int_{\eta_1}^{\eta_2} d\eta (\xi^2 + \eta^2 + 1)^{-\frac{1}{2}} \left\{ c_1 + c_2 \left[1 - (\xi^2 + \eta^2 + 1)^{-\frac{1}{2}}\right]^2 \right\}$$

$$\times \exp\left[-A_\Sigma (\xi^2 + \eta^2 + 1)^{\frac{1}{2}}\right], \quad \alpha = +\frac{\pi}{2}, \tag{4.38}$$

derived the same way as eq. (4.34), we find

$$E_{\Sigma_0} = \left[-c_1 \left\{ y^{-1} \exp(-a_\Sigma y) + a_\Sigma E_1(a_\Sigma y) \right\} - c_2 \left\{ y^{-1} \exp(-a_\Sigma y) \right.\right.$$

$$\times \left[(1 + a_\Sigma + \tfrac{1}{6} a_\Sigma^2) - (1 + \tfrac{1}{6} a_\Sigma) y^{-1} + \tfrac{1}{3} y^{-2} \right]$$

$$\left. \left. + (1 + a_\Sigma + \tfrac{1}{6} a_\Sigma^2) a_\Sigma E_1(a_\Sigma y) \right\} \right]_{y=1}^{y = \sec \theta_1}. \tag{4.39}$$

29

C. Approximation of the Reduction Factor.

The general approximate form for R is

$$R \simeq R_o \equiv \sum B_{oi} E_{\Sigma_{oi}} \qquad\qquad (4.40)$$

In most cases the Σ_o choices described in this section and the last, e.g. the centered approximation, are adequate approximations to Σ, giving results which are off only by a few percent. But Figure 8 shows an example in which the centered approximation to a rectangular representation of a slab Σ entails a sizable distortion. Here we may retain eq. (3.35), but change the values of the v_i so that cancellation in E_{Σ_o}, of errors from portions of Σ near the middle of and exterior to Σ_o, with errors at the corners, in Σ_o but exterior to Σ can occur. This results in v_i slightly smaller in absolute value than values stemming from eq. (3.36). The best values of v_1, for example, can be estimated by equating the ratio of the areas of the (right) "triangles" with centroids A and B in the figure to the values of the integrand of E_Σ at these two points. This condition gives the base of triangle A, which determines v_1. This is the method we have used to improve the choice of Σ_o for the long side walls of the M113 in the next section. For identification purposes we call this the "reshaping approximation".

5. "WALLS ONLY" MODEL OF THE M113.

In the phrase "walls only" we intend that the floor and ceiling surfaces also be included. Figure 8 shows the indexing convention for the surfaces of the M113. To achieve the idealization implied by the contents of the figure we have identified the inner framing plates with the hull walls, ignored a variety of surface bumps and irregularities, and represented the sides of the vehicle as flat. Figure 9 is a sketch of the vehicle cross section as seen from the rear, together with some aspects of the idealization implied by our procedure.

We choose the detector position to be 30 inches above the floor, or 45.9 inches above the ground, so that h_{eff} = (36 + 45.9) in = 6.8 ft, and x = .0158. The detector is centered, equidistant from the two sides, and also more or less is centered with respect to front and rear, beneath the cupola opening. In Table 1 we list the data for each of the Σ_i, much of which partially is determined by choice of detector position. In Table 2 we list the computed values of the* $E_{\Sigma_{oi}}$, the buildup factors, and the $r_{\Sigma_{oi}}$.

By a process of inspired scrutiny involving eq. (3.30) we have estimated crudely a 1.05 refraction correction; also, we assume a 10% albedo, so that from eq. (4.40) and Table 2,

$$\mathcal{R} = 1.155R = .6521 \tag{5.1}$$

$$P = \mathcal{R}^{-1} = 1.53 \tag{5.2}$$

---

* For Σ_6 (Σ_7) we have computed E_{Σ_o} for the detector position above (below) the center of Σ_6 (Σ_7) for simplicity. This is almost exaxtly the case for Σ_6 so the error here is small; it is greater for Σ_7, but this is tolerable because the total skyshine contribution is small, anyway.

Also we have divided Σ_1 ($=\Sigma_2$) into $\Sigma_1^\uparrow + \Sigma_1^\downarrow$, where $\Sigma_1^\uparrow$ is the portion of Σ_1 above the horizontal plane containing the detector and $\Sigma_1^\downarrow$ the portion below. For $\Sigma_1^\uparrow$ we have taken $u_1 \neq u_2$ to take account of the shape irregularity. By the remark in paragraph 1 of Section 4, $E_{\Sigma_1^\uparrow} = \frac{1}{2}(E_{\Sigma_{1L}^\uparrow} + E_{\Sigma_{1R}^\uparrow})$ where L and R refer to the left $(u = u_1)$ and right $(u = u_2)$ portions of $\Sigma_1^\uparrow$.
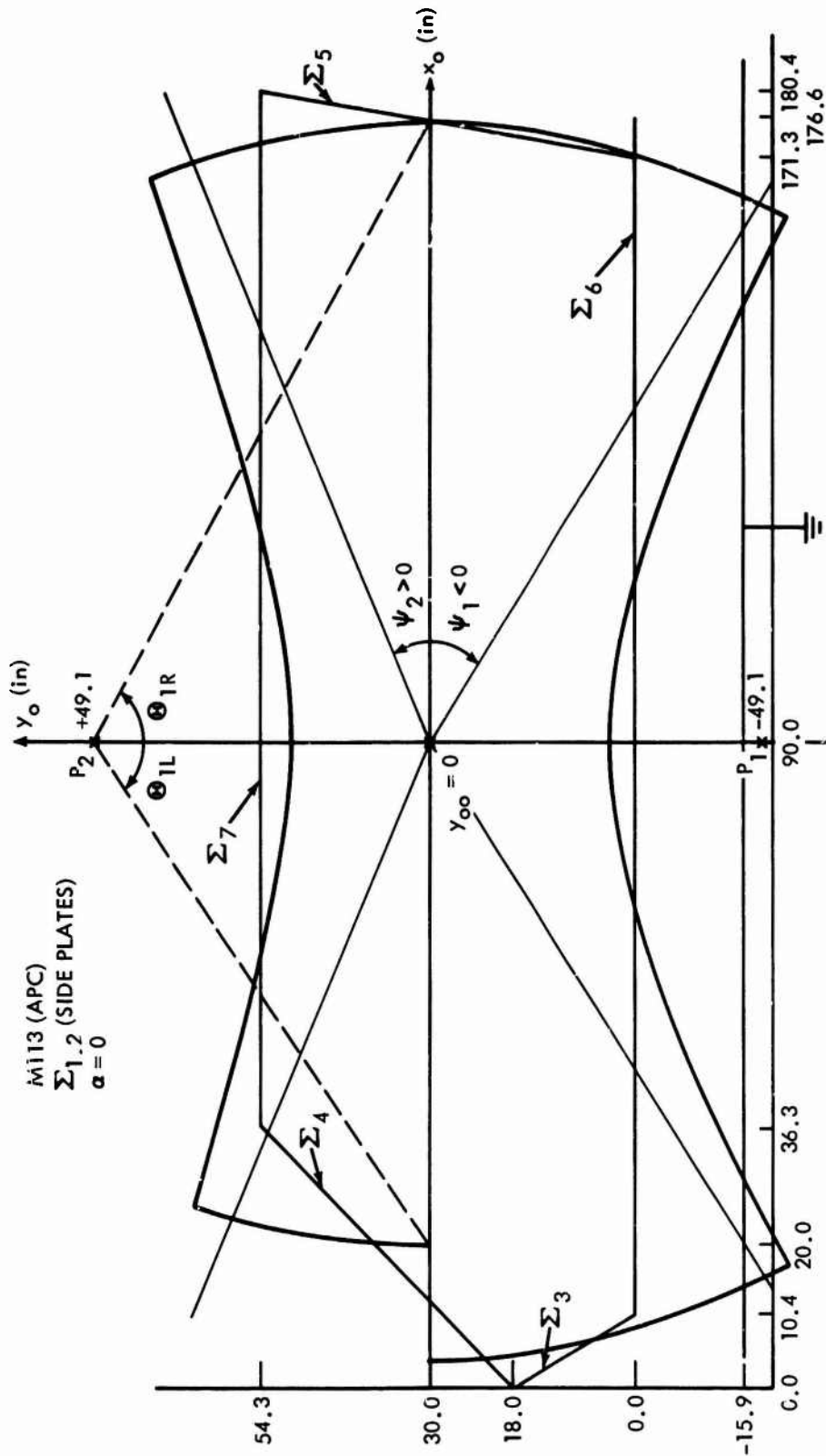
FIG. 8 "Reshaping approximations" to the rectangles used to represent the M113 surface $\Sigma_1 = \Sigma_1^{\downarrow} + \Sigma_1^{\uparrow}$. u_1 and u_2 are chosen the same way as in the centered approximation (FIG. 6 and 7), but v_1 and v_2 are chosen differently, as described in the text. The necessity arises from the fact that the dimensions of the slab are big, in relation to $P_1P_2 = 2D = 2z_1 \sec \alpha$. The illustration also shows the indexing convention for the remaining surfaces of the M113.
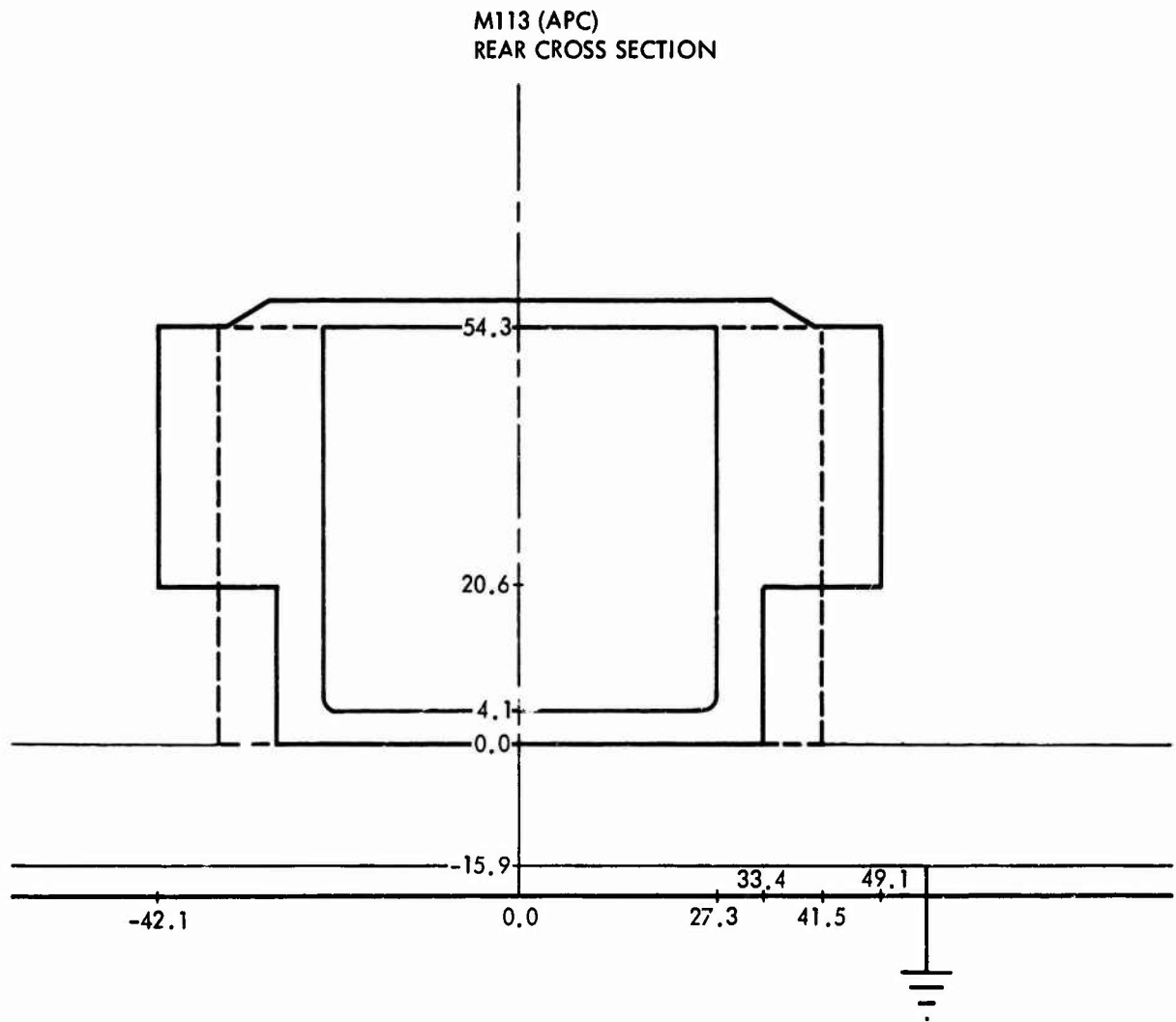
M113 (APC)
REAR CROSS SECTION

FIG. 9 M113 vehicle cross section, from the rear, showing the double wall structure.
The dotted lines trace out the rectangular cross section for the "walls only" model.

	$\Sigma_1^{\downarrow}=\Sigma_2^{\downarrow}$	$\Sigma_1^{\uparrow}=\Sigma_2^{\uparrow}$	Σ_3	Σ_4	Σ_5	Σ_6	Σ_7
α	0	0	$-9.854°$	$+45°$	$-30°$	$-90°$	$+90°$
t	1.875	1.875	1.500	1.500	1.500	1.500	1.625
z_1	49.1	49.1	84.7	55.2	83.9	30.0	24.3
x_1, x_2	86.0	70.0, 86.0	49.1	49.1	49.1	83.1	72.1
y_1	-30.0	0	-15.7	-72.1	+13.8	-49.1	-49.1
y_2	0	+24.3	+59.4	-20.8	+34.6	+49.1	+49.1
u_1, u_2	2.02	1.74, 2.02	1.1516	1.1816	1.1211	---	---
v_1	-.520	0	-.3539	-.2164	-.3575	---	---
v_2	0	+.420	+.2871	+.4407	-.1428	---	---
Θ_1, Θ_2	1.0495	.9580, 1.0495	.5189	.5620	.4691	---	---
ψ_1	-.547	0	-.3618	-.218	-.3656	---	---
ψ_2	0	+.433	+.2912	+.456	-.1433	---	---

Table 1. Slab data for computing the M113
protection factor in the "walls only"
model. Entries for dimensioned quantities,
in rows 2 - 6, all are expressed in inches;
entries in the last three rows, 10 - 12,
are in radians.

	$\Sigma_1^{\downarrow}=\Sigma_2^{\downarrow}$	$\Sigma_1^{\uparrow}=\Sigma_2^{\uparrow}$	Σ_3	Σ_4	Σ_5	Σ_6	Σ_7
E_{Σ_0}	.0873	.0114	.0516	.0272	.0101	.0766	.0144
B_0	1.548	1.548	1.438	1.438	1.438	1.438	1.475
r_{Σ_0}	.1351	.0176	.0742	.0391	.0145	.1102	.0212

Table 2. Attenuation, buildup, and reduction factors for the surfaces of the "walls only" model of the M113.

From eq. (2.6), using L(6.8 ft.) = .86 we find

$$S = 1.32, \tag{5.3}$$

which is considerably smaller than the average value reported in Reference 1,

$$S = 3.41, \tag{5.4}$$

where variations of detector position did not involve deviations of more than 10 to 15%.

The results of the simplified model of Section 6 support the hypothesis that the discrepancy between (5.3) and (5.4) is due to neglect of shielding effects from material present additionally to that which resides in the vehicle's surfaces.

6. PARALLELIPIPED MODEL

The combat loaded weight of the M113 is 24,000 pounds[7] while the weight of material assumed for the calculation of Section 5 is

$$W_{shell} = \rho_{Al} \sum_i A_i t_i \qquad (6.1)$$

where $\rho_{Al} = 2.72\rho_{H_2O} = 2.72 \times 62.4 \ \#/ft^3 = 117 \ \#/ft^3$, the density of Aluminum, A_i is the area of Σ_i, and t_i its thickness. The volume factor in eq. (6.1) for the M113 is

$$\sum_i A_i t_i = 57.96 \ ft^3 \quad (M113) \qquad (6.2)$$

so that $W_{shell} = 9838^\#$, which is only 41% of the combat loaded weight given above. In light of this, the disagreement between (5.3) and (5.4) is hardly unreasonable. We proceed to a simplified model and calculation for the M113, based on the information and experience gained so far.

We idealize the vehicle by a closed shell of uniform thickness and (possibly heterogeneous) composition. The attenuation constant for the unscattered component of the radiation due to atoms of species k is

$$\mu_k = n_k \sigma_k \qquad (6.3)$$

when n_k is the number density for atoms of species k and σ_k the corresponding γ-ray cross section. We define an effective thickness,

$$t_{eff} = W/(\rho_{Al} A), \qquad (6.4)$$

where W is the total weight of the fully loaded vehicle and A is the surface area of the shell used to model it. Then the unscattered component penetrating the wall is proportional to

$\exp(-\bar{\mu} t_{eff})$, where

where

$$\bar{\mu} = (\sum_k \mu_k t_k) t_{eff}^{-1} \qquad (6.5)$$

$$= \mu_{Al} \sum_k f_k g_k, \qquad (6.6)$$

with

$$f_k = W_k/W \qquad (6.7a)$$

$$g_k = (Z/A)_{Al}^{-1} (Z/A)_k, \qquad (6.7b)$$

wherein W_k is the weight of material of species k, Z is the number of electrons on the indicated atom and A the corresponding atomic weight.

The composition of the M113 was not available to us, so to estimate $\bar{\mu}$ we have modeled the material breakdown as follows:

Aluminum	10,000#
Fuel	2,000#
13/160# dummies	2,100#
Other	9,900#
Total	24,000#

The "other" entry includes the motor, hatches, gun, treads, etc., of which we assume about 2/3 to be iron, with specific gravity = 7.86, and the rest aluminum. The results, together with the values assumed or computed for the f_k and the g_k, are given in Table 3. The result is

$$\bar{\mu}/u_{A\ell} = 1.02$$

so we just take

$$\bar{\mu} = \mu_{A\ell} \tag{6.8}$$

as the attenuation constant for the shell wall, and

$$t = t_{eff} \tag{6.9}$$

as its thickness.

In the present model we have concentrated all the material present into the shell, disregarding effects of the actual, quite complicated, distribution of matter. In the same spirit we choose the simplest shape to work with, a parallelepiped having a square vertical cross section of side L, and a height H equal to that of the actual vehicle. We fix L by equating the surface area of the square parallelepiped to that of the best rectangular/parallelepiped representation of the vehicle's actual shape, which we estimate from the Master Diagram[6]:

$$\left.\begin{array}{lll} \text{length} & = & 162.3 \text{ in.} \\ \text{width} & = & 83.0 \text{ in.} \\ \text{H} & = & 54.3 \text{ in.} \end{array}\right\} \quad \text{(M113)} \tag{6.10}$$

This gives $A = 372 \text{ ft}^2$, $t_{eff} = 4.56$ in., $L = 118.1$ in.

Species	Sp. Grav.	W_k (#)	f_k	g_k
Aluminum	2.7	13,400	.56	1.00
Iron	7.86	6,500	.27	.95
Dummies	1.8	2,100	.09	1.10
Fuel	1.0	2,000	.08	1.23

Table 3. Estimated material breakdown for the M113.

For all the walls $\alpha = 0$, so we may use eq. (4.21). We compute just the direct contribution $R^{(d)}$ to R, correcting for skyshine and albedo together by multiplying by 1.1 (skyshine) x 1.1 (albedo) = 1.21;

$$\mathcal{R} = 1.21\ R^{(d)}, \tag{6.11}$$

where

$$R^{(d)} = B_o(t_{eff})\,(E_f + \sum_{i=1}^{4} E_{w_i}^{(d)}), \tag{6.12}$$

with suffixes $\underline{f}$ and $\underline{w}$ referring to floor and wall, with $B_o(t_{eff})$ given by eq. (2.27), and with

$$E_{w_i}^{(d)} \doteq \frac{1}{\pi}(J_1^{(d)} I_1(o))_i. \tag{6.13}$$

We place the detector on the vertical axis through the center of the square so all the $E_{w_i}^{(d)}$ are equal; this also makes Σ_o a circle for the floor slab. For the wall we assume the centered approximation, eqs. (3.35) and (3.36). We assume the detector to be at a height h_f above the floor. Collecting all the necessary formulas specialized to this case we have:

$$P^{-1} = \mathcal{R} = 1.21\ R^{(d)} \tag{6.14a}$$

$$R^{(d)} = B_o(t_{eff}) \cdot (E_f + 4\ E_w^{(d)}) \tag{6.14b}$$

$$B_o(t_{eff}) = 1 + .292\ t_{eff}\ (in) \tag{6.14c}$$

$$E_f = c(E_1(A) - E_1(A \sec \theta_1)) \tag{6.14d}$$

$$A = a_\Sigma + \varkappa, \quad a_\Sigma = \mu_{A\ell} t_{eff} \tag{6.14e}$$

$$\varkappa = .002314 (ft)^{-1} \cdot (h_f + 15.9 \text{ in} + 3 \text{ ft}), \tag{6.14f}$$

$$\sec \theta_1 = (1 - w_f)^{-1} \tag{6.14g}$$

$$\omega_f = 2\pi^{-1} \tan^{-1} \xi_{2f}^2 (1 + 2\xi_{2f}^2)^{-\frac{1}{2}} \tag{6.14h}$$

$$\zeta_{2f} = L/(2h_f) \tag{6.14i}$$

$$E_w^{(d)} = \pi^{-1} J_1^{(d)} I_1(0) \tag{6.14j}$$

$$I_1(0) = S(a_\Sigma, \Theta_2 = 45°) \tag{6.14k}$$

$$J_1 = cE_1(\zeta_1), \quad c = .2034 + .783\varkappa, \tag{6.14\ell}$$

$$\zeta_1 = -\varkappa v_1^{-1} \tag{6.14m}$$

$$v_1 = -2h_f/L \tag{6.14n}$$

The sources, respectively, are eqs. (2.5) and (6.10), (6.11),
(2.27), (4.37), (4.35) and (3.29), (2.8) and (2.22) (with $h = h_f + 15.9$
in. replaced by $h + \Delta h$, $\Delta h = 3$ ft ground roughness, and where 15.9
is the height above ground of the floor slab), (4.32), (4.10) and
(4.12), (3.11), (4.21), (3.35) and (4.22), (4.27b) and (2.25),
(4.26), and (3.36).
We have not included a refraction correction here as we did in
Section 5 (cf. eq. (5.1) since the magnitude of the effect, which is
the "softening" of the unscattered attenuation at large θ_c, is well
overshadowed by that arising from the irregularities of the actual
mass distribution. Also, the neglect of shape effects implied by
the assumption of square vertical cross section renders such a
consideration doubtful. Finally, a 5% correction can be absorbed
by modelling the vehicle so that L is a little smaller; for the
M113, changed, slightly smaller, dimensions of the "best" rectangular
parallepiped representation of the vehicle's actual shape involve
estimates as reasonable as those given in (6.10). A similar remark
holds for the P7.

We see from eqs. (6.14) that P and $\hat{R}$ are fixed as functions of
h_f when t_{eff} and L are given, as, e.g., in (6.10) for the M113. The
answers, for two choices of detector height, h_f, above the floor of
the vehicle, are

$$\mathcal{R} = \mathcal{R}(h_f) = .2734 \qquad h_f = 25.9 \text{ in.} \left.\right\}$$
$$= .2544 \qquad h_f = 45.9 \text{ in.} \left.\right\} \qquad (6.15)$$

so that

$$P(25.9 \text{ in.}) = 3.66 \left.\right\}$$
$$P(45.9 \text{ in.}) = 3.93 \left.\right\} \qquad (6.16)$$

and, by eq. (2.6), $S = .86\ P$,

$$S(25.9 \text{ in.}) = 3.15 \left.\right\}$$
$$S(45.9 \text{ in.}) = 3.38 \left.\right\} \qquad . \qquad (6.17)$$

From Reference 1, for positions 18 in from the (two) side walls, experiment gives

$$S(47.25 \text{ in.}) = 3.59,\ 3.07 \left.\right\}$$
$$S(49.25 \text{ in.}) = 3.76,\ 3.24 \left.\right\} \qquad (6.18a)$$

which gives an idea of the experimental spread arising from the matter distribution. The average of these values of S is 3.42, suggesting

$$S(48.25 \text{ in.}) = 3.4 \pm .3. \qquad (6.18b)$$

Experiment also gives, 27 in. from the left wall,

$$S(31 \text{ in.}) = 3.61, \qquad (6.18c)$$

a value within the indeterminacy* indicated in (6.18b). Comparing these values with our computed result, eqs. (6.17), we see that the agreement is good. ("Too good", of course; a 15% albedo weakens the agreement by 5%.)

Turning to the marine corps LVTP7, we take[8]

$$\begin{aligned}
\text{length} &= 293.0 \text{ in.} \\
\text{width} &= 103.6 \text{ in.} \\
H &= 78.0 \text{ in.}
\end{aligned} \left.\right\} \quad (P7) \qquad (6.19)$$

which gives $A = 851 \text{ ft}^2$, $t_{eff} = 4.33$ in, $L = 181.6$ in, and

$$h_f = 25.9 \text{ in.:} \quad \mathcal{R} = .2562,\ P = 3.90,\ S = 3.35 \left.\right\}$$
$$h_f = 45.9 \text{ in.:} \quad \mathcal{R} = .2471,\ P = 4.05,\ S = 3.48 \left.\right\} \qquad . \qquad (6.20)$$

---

*As distinguished from "uncertainty!"

We adopt for the residual radiation transmission factor (RRTF) the following:

$$M113: \quad RRTF = S^{-1} = (3.4)^{-1} = .29 \text{ experiment}$$
$$S^{-1} = (3.5)^{-1} = .29 \text{ theory} \tag{6.21}$$
$$P7: \quad RRTF = S^{-1} = (3.7)^{-1} = .27 \text{ theory.} \tag{6.22}$$

Accordingly we recommend the adoption of the value

$$RRTF = .3 \qquad \qquad (LVTP7). \tag{6.23}$$

7. DISUCSSION

The RRTF for both vehicles is 0.3 despite the fact that the P7 weighs more than twice as much as the M113. Note, however, that t_{eff}^{M113} = 4.56 in and t_{eff}^{P7} = 4.33 in, so the model wall thickness, which is a principal determining factor, is nearly the same for the two cases. This reflects the fact that the extra weight is a size effect, L^{M113} = 118.1 in and H^{M113} = 54.3 in. being somewhat less than the corresponding values for the P7, L^{P7} = 181.6 in. and H^{P7} = 78.0 in. Moreover, since the floors of both vehicles are 15.9 in. from the ground, equal values of h_f and h mutually imply each other; and since H^{P7} > H^{M113}, proportionately more of the total mass of the P7 than of the M113 lies above the horizontal plane through the detector position. This means that much of the P7's added mass is positioned so that it protects only against the relatively ineffectual skyshine "threat" ($\theta > \pi/2$).

8. SUMMARY AND CONCLUDING REMARK

We have computed the residual radiation transmission factor for the Marine Corps LVTP7 to be 0.3, based on a model of the mass distribution whose results for application to a similar vehicle, the army APC M113, agree with experiment.

We have accomplished this by developing a new analytical approximation scheme for transmission through a rectangular (wall) slab. The scheme has a wide range of applications, to the case where the plane of the slab is not too close to the horizontal: specifically, $|\alpha|$ not too close to $\cos^{-1}\varkappa$. The method employs the approximation that the conics determined by the intersection of the cones of constant θ with the plane of the slab coincide with the hyperbolic arcs of a natural elliptical coordinate system in the plane of Σ. The coordinate system is chosen by requiring the conic determined by $\cos\theta = \varkappa$, along which the source angular distribution maintains its peak value, to coincide with the corresponding hyperbolic arc. Finally, Σ is replaced by an approximation, Σ_o, more convenient for calculation: the boundaries of Σ_o are segments of ellipses (sides) and hyperbolas (top and bottom) "parallel" to the curvillinear axes of the natural coordinate system for the problem.

We remark, finally, that the use of natural coordinates should simplify mesh size problems encountered in programming the surface integrals for numerical integration, at a considerable savings in computer time and cost. Small mesh sizes can be chosen for the v-integration, probing the rapid variation of the source function through the peak near $\cos\theta = \varkappa$, and large mesh sizes will suffice for the v-integration since the v-dependence of the integrand is relatively weak.

REFERENCES

1. M. J. Schumchyk, R. E. Rexroad, M. A. Schmoke, and W. C.
   Hampton, "Fallout Shielding Characteristics of Combat Vehicles
   M60 and M48A2 Tanks, M59 and M113 Armored Personnel Carriers,"
   U. S. Army NDL-TR-45, Edgewood Arsenal, September 1965;
   M. A. Schmoke, R. E. Rexroad, and M. J. Schumchyk, "Evaluation
   of Internal Radiac Detector Positions for the M48A2 Tank and
   the M113 Armored Personnel Carriers," U. S. Army NDL-TR-52,
   Edgewood Arsenal, June 1966.

2. L. V. Spencer, "Structure Shielding against Fallout Radiation
   from Nuclear Weapons," NBS Monograph 42, National Bureau of
   Standards, Gaithersburg, Maryland, June 1, 1962.

3. "Engineering Compendium on Radiation Shielding," Vol. I, R. G.
   Jaeger, E. P. Blizard, A. B. Chilton, M. Grotenhuis, A Honig,
   Th. A. Jaeger, H. H. Eisenlohr, eds. (Article 4.3.1.2 "Buildup
   Factor," by A. B. Chilton) Springer-Verlag, New York, 1968,
   pp 210 & ff.

4. W. Heitler, "The Quantum Theory of Radiation," 3rd ed. (Oxford,
   1954) p. 221.

5. National Bureau of Standards Applied Mathematical Series - 55,
   "Handbook of Mathematical Functions," Milton Abramowitz and
   Irene A. Stegun, eds., Gaithersburg, Md., November, 1964, p. 1000.

6. Master Diagram, APC M113, FMC Corporation, Ordnance Division,
   San Jose, California, Drawing No. 1045154.

7. M. A. Schmoke (private communication).

8. Master Diagram, LVT EX3, FMC Corporation, Ordnance Division,
   San Jose, California, Drawing No. 4168350.